Journal of Structural Engineering. Submitted April 12, 2011; accepted May 3, 2013;
posted ahead of print May 6, 2013. doi:10.1061/(ASCE)ST.1943-541X.0000863

LATERAL FORCE-DISPLACEMENT RESPONSE OF UNREINFORCED MASONRY WALLS WITH FLANGES

By A. P. Russell, S.M.ASCE[1], K. J. Elwood, M.ASCE[2] and J. M. Ingham, M.ASCE[3]

ABSTRACT

The experimental in-plane force-displacement response of unreinforced masonry (URM) walls with flanges (return walls) subjected to pseudo-static cyclic lateral loading is presented. Each wall failed in a diagonal tension mode followed by bed-joint sliding. The effect of wall flanges was to increase the displacement capacity of the in-plane loaded wall, when compared with an in-plane loaded wall without flanges. The measured shear strengths of the walls were compared with an analytical model for determining the limiting diagonal tension strength of walls, with a high level of correlation. The initial stiffness of the shear walls before effective yield was compared with the initial stiffness as determined using conventional principles of mechanics for homogeneous materials, and it was found that with some approximations the initial stiffness could be satisfactorily determined. Because the bed-joint sliding failure mechanism exhibited by the walls is a deformation-controlled action, there is further displacement capacity beyond the effective yield displacement, and it was found that the walls could sustain in-plane lateral forces to

[1] Cement & Concrete Association of New Zealand, P.O. Box 448, Wellington 6140, New Zealand, E-mail: arus033@aucklanduni.ac.nz

[2] Associate Professor, Department Of Civil Engineering, The University of British Columbia, Vancouver, BC V6T 1Z4, Canada, E-mail: elwood@civil.ubc.ca

[3] Professor, Department of Civil and Environmental Engineering, The University of Auckland, Private Bag 92019, Auckland 1142, New Zealand, E-mail: j.ingham@auckland.ac.nz

Journal of Structural Engineering. Submitted April 12, 2011; accepted May 3, 2013;
posted ahead of print May 6, 2013. doi:10.1061/(ASCE)ST.1943-541X.0000863

a drift of at least 0.7%. Recommendations are provided for a general force-displacement relationship which is consistent with the experimental data and can be used for modelling URM walls and improving acceptance criteria, such as those specified in ASCE/SEI 41-06.

CE DATABASE SUBJECT HEADINGS: Masonry, Seismic effects, Cyclic load, Shear walls, Shear strength.

Journal of Structural Engineering. Submitted April 12, 2011; accepted May 3, 2013;
posted ahead of print May 6, 2013. doi:10.1061/(ASCE)ST.1943-541X.0000863

INTRODUCTION

Many unreinforced clay brick masonry buildings can be expected to sustain significant damage when subjected to strong ground motion. The construction of such buildings was common in the early part of the 20th Century in New Zealand, Canada, and the United States when structural design philosophies were focused on gravity loading, with little thought given to the lateral force resistance of URM walls or lateral load demands from earthquakes (Russell and Ingham, 2010). Consequently in many countries URM buildings commonly form a significant part of both the heritage building stock and the building stock considered most vulnerable to earthquake damage. This vulnerability was clearly evident from the damage to URM buildings resulting from the M7.1 2010 Darfield (Dizhur et al., 2010; Ingham and Griffith, 2011) and the M6.3 2011 Christchurch earthquakes (Ingham et al., 2011).

Considerable experimental and analytical research has focused on the in-plane response of rectangular URM walls (e.g., Atkinson et al. (1989), Abrams (1997), Gambarotta and Lagomarsino (1997b; 1997a), Steelman and Abrams (2007)). However, it has been identified in the literature (Moon et al., 2006; Yi et al., 2006a,b, 2008) that codified equations for assessing the strength and displacement capacity of URM walls loaded in-plane (e.g. ASCE/SEI 41-06, 2007) are overly conservative, particularly when assessing URM walls with flanges (return walls). Consequently, the objective of this research was to investigate the lateral in-plane response of flanged URM walls, in the context of previous research into failure modes, and to determine strength and displacement limits.

Journal of Structural Engineering. Submitted April 12, 2011; accepted May 3, 2013;
posted ahead of print May 6, 2013. doi:10.1061/(ASCE)ST.1943-541X.0000863

Flanges are defined by Moon et al. (2006) as the portion of the out-of-plane wall that participates with the in-plane wall to resist lateral loads. Yi et al. (2008) noted that previous experimental research on URM building systems (Costley, 1996; Paquette and Bruneau, 2003; Moon et al., 2006; Yi et al., 2006b) has highlighted the beneficial effects of flanges on the response of in-plane loaded walls and indicated the potential for flanges to influence wall failure modes and maximum strength. Yi et al. (2008) also noted that no experimental data were available which specifically investigated the seismic (lateral) performance of individual flanged URM walls. Following full scale testing of a two storey URM building (Moon, 2004; Yi, 2004; Yi et al., 2006b; Yi et al., 2006a) where significant flange participation on in-plane wall response was observed, Yi et al. (2008) developed an analytical model to investigate the effects of flanges on the behaviour of individual non-rectangular section URM piers. It was also postulated by Yi et al. (2008) that the drift corresponding to lateral-load failure is dependent on the location of the flange in relation to the in-plane wall. When the flange is at the toe of the wall (the flange is in compression), it was postulated that the flange reduces the compressive stress at the toe and delays toe crushing failure. Conversely, it was postulated that when the flange is at the heel (in tension) the compressive stress in the toe increases due to the increased weight of the flange. The current study was conducted to address the paucity of experimental data on flanged URM walls, validate the models proposed by Yi et al. (2008), and develop recommendations for the lateral force–displacement response of URM walls with flanges.

Journal of Structural Engineering. Submitted April 12, 2011; accepted May 3, 2013;
posted ahead of print May 6, 2013. doi:10.1061/(ASCE)ST.1943-541X.0000863

BACKGROUND

The following sections provide background on failure mode definitions, strength and stiffness models, and drift capacities for in-plane URM walls.

Failure Modes

Failure modes of unreinforced masonry piers subjected to combined gravity and seismic actions can be generally classified as either deformation-controlled or force-controlled ASCE/SEI 41-06 (2007). Deformation-controlled elements have some displacement capacity beyond the point of effective yield, but force-controlled elements respond in a brittle manner, and have no further capacity beyond when the maximum force is attained. Figure 1 shows a general force-deformation response for URM walls responding in-plane as considered by ASCE/SEI 41-06 (2007). Figure 1(a) corresponds to deformation-controlled masonry elements and Figure 1(b) corresponds to force-controlled masonry elements.

In total, six URM failure modes are outlined in various publications, but the definition of each mode differs (see Table 1). Yi et al. (2008), FEMA 356 (2000) and FEMA 273 (1997) suggest four failure modes. Bed-joint sliding and rocking are deformation-controlled mechanisms, and diagonal tension and toe crushing are force-controlled actions. No distinction is made between sliding along a single continuous bed-joint and stair-stepped sliding along bed-joints in different courses, and similarly no distinction is

Journal of Structural Engineering. Submitted April 12, 2011; accepted May 3, 2013;
posted ahead of print May 6, 2013. doi:10.1061/(ASCE)ST.1943-541X.0000863

made between diagonal tension failure with cracks occurring through the bricks or through the mortar joints. ASCE/SEI 41-06 (2007), which has replaced FEMA 356 (2000), gives strength limits for only three of the above failures modes, and eliminates diagonal tension as a failure mode. That is, ASCE/SEI 41-06 (2007) does not recognise that such a failure could occur. Moreover, rocking is the only failure mode considered to be deformation-controlled (with associated drift limits), and the equation formerly used in FEMA 356 for bed-joint sliding shear is given to determine the "lower-bound shear strength for the wall or pier". In ASCE/SEI 41-06 (2007) the wall is considered to be force-controlled, unless the expected strength of the URM wall is limited by rocking. Hence, from FEMA 356 (2000) to ASCE/SEI 41-06 (2007), the treatment of sliding shear changed from a deformation-controlled failure mode (with associated drift limits) to a force-controlled failure mode.

The appropriate sections relating to URM in NZSEE (2006) are based largely on information provided in Magenes and Calvi (1997). Four failure modes are proposed, but do not correspond directly with the failure modes in Yi et al. (2008) or FEMA 356 (2000). Rocking and toe crushing are not differentiated, and are termed a "flexural failure". Sliding on a single continuous bed-joint is considered to be a failure mode. Diagonal tension is differentiated according to whether the cracks occur through the bricks or through the mortar joints (around the bricks). Diagonal tension cracking occurs due to the principal tension stress σ_1 exceeding the diagonal tension strength of the masonry f_{dt}. Magenes and Calvi (1997) term this behaviour simply as "shear cracking" and state that "peak resistance is governed by the formation and development of inclined

Journal of Structural Engineering. Submitted April 12, 2011; accepted May 3, 2013;
posted ahead of print May 6, 2013. doi:10.1061/(ASCE)ST.1943-541X.0000863

diagonal cracks, which may follow the path of bed- and head-joints or may go through the bricks, depending on the relative strength of mortar joints, brick-mortar interface, and bricks." When the mortar much is weaker than the bricks, the cracking can be expected to occur in a step-wise manner. Derakhshan et al. (2010), Dizhur et al. (2009) and Dizhur and Ingham (2010) note that for existing URM buildings in New Zealand the quality of mortar is usually poorer than the quality of bricks, and as such, cracking through the mortar joints is more likely. This conclusion is also supported from general observations following the M7.1 Darfield and M6.3 Christchurch earthquakes (Dizhur et al., 2011). Although not directly acknowledged in any of the publications shown in Table 1, diagonal tension failure with cracking through the mortar joints is often followed by stair-stepped bed-joint sliding. In the case when the mortar is stronger than the bricks, cracking due to diagonal tension will occur through the bricks, and there will not be further displacement capacity beyond the point where cracking occurs. This form of diagonal-tension failure is clearly consistent with the definition of a force-controlled mechanism.

Models for Predicting In-Plane Wall Strength

The Yi et al. (2008) models considered in this study for determining the behaviour of walls responding in-plane, including the influence of flanges, are summarised in Equations (1) – (4),

$$V_s = \frac{\mu N + 3a_i b_w v_{me}}{1 + \frac{3h_{eff} b_w v_{me}}{N}} \quad (1)$$

Journal of Structural Engineering. Submitted April 12, 2011; accepted May 3, 2013;
posted ahead of print May 6, 2013. doi:10.1061/(ASCE)ST.1943-541X.0000863

$$V_{tc} = \frac{N}{h_{eff}} l_w \left(\frac{a_i}{l_w} - \frac{2}{3} \frac{N}{\beta f_m l_w b_w} \right) \tag{2}$$

$$V_{dt} = \frac{b_w l_w f_{dt}}{\zeta} \sqrt{1 + \frac{f_m}{f_{dt}}} \frac{\left(1 + \frac{W_f}{W_w}\right)\left(\frac{1}{6}\left(1 + \frac{W_f}{W_w}\right) + \frac{1}{2}\frac{W_f}{W_w}\right)}{\left(\frac{W_f}{W_w} + \frac{1}{2}\right)^2} \tag{3}$$

$$V_r = \frac{N}{h_{eff}} \frac{\left(\frac{l_w b_w a_i}{2} - \frac{l_w^2 b_w}{6} + (a_i - a_f) A_f \left(1 - \frac{a_f}{l_w}\right) \right)}{\left(\frac{l_w b_w}{2} - A_f \right)} \tag{4}$$

where V_s, V_{tc}, V_{dt} and V_r are the lateral strength of the URM wall corresponding to sliding, toe crushing, diagonal tension and rocking, respectively; β is a factor to account for nonlinear vertical stress distribution and has a value β=1.3 from Yi et al. (2005), and ζ is a factor to account for wall aspect ratio, which Benedetti and Tomaževič (1984) proposed as ζ=1 for $h/l_w \leq 1$, $\zeta = h/l_w$ for $1 < h/l_w < 1.5$, ζ=1.5 for $h/l_w \geq 1.5$. Equation (1) does not differentiate between sliding on a single continuous bed-joint and sliding in a stair stepped pattern, and Equation (3) does not define whether diagonal tension causes cracking through or around the bricks.

NZSEE (2006) provides strength limits based on sliding shear V_s, diagonal tension failure due to damage in mortar joints V_j, diagonal tension failure due to cracking through bricks V_b, and flexural resistance V_r (rocking):

$$V_s = \frac{3czb_w + \mu N}{1 + \frac{3cl_w b_w \alpha_c}{N}} \tag{5}$$

$$V_j = \frac{cl_w b_w + \mu N}{1 + \alpha_c} \tag{6}$$

Journal of Structural Engineering. Submitted April 12, 2011; accepted May 3, 2013;
posted ahead of print May 6, 2013. doi:10.1061/(ASCE)ST.1943-541X.0000863

$$V_b = \frac{\sqrt{f_{bt} l_w b_w (f_{bt} l_w b_w + N)}}{2.3(1+\alpha_c)} \tag{7}$$

$$V_r = \frac{N}{h_{eff}}\left(z - \frac{1}{2}\frac{N}{0.85 f'_m\, b_w}\right) \tag{8}$$

The predicted strength using FEMA 356 (2000) is given in Equations (9) – (12), for bed-joint sliding V_{bjs}, toe crushing V_{tc}, diagonal tension V_{dt} and rocking V_r. In ASCE/SEI 41-06 (2007), Equation (11) is not included and Equation (9) is referred to the "lower-bound shear strength for wall or pier" instead of "bed-joint sliding shear".

$$V_{bjs} = v_{me} A_n \tag{9}$$

$$V_{tc} = \alpha N \frac{l_w}{h_{eff}}\left(1 - \frac{f_m}{0.7 f'_m}\right) \tag{10}$$

$$V_{dt} = v_{me} A_n \frac{l_w}{h_{eff}}\sqrt{1 + \frac{f_m}{v_{me}}} \tag{11}$$

$$V_r = 0.9 \alpha N \frac{l_w}{h_{eff}} \tag{12}$$

Initial Stiffness

ASCE/SEI 41-06 (2007) suggests Equation (13) for calculating the lateral in-plane stiffness of a solid cantilevered shear wall, K_{ic}, and A_v is determined from Equation (14).

$$K_{ic} = \frac{1}{\frac{h_{eff}^{\ 3}}{3E_m I_{eff}} + \frac{h_{eff}}{A_v G_{eff}}} \tag{13}$$

Journal of Structural Engineering. Submitted April 12, 2011; accepted May 3, 2013;
posted ahead of print May 6, 2013. doi:10.1061/(ASCE)ST.1943-541X.0000863

$$A_v = b_{w,eff} \cdot l_{w,eff} \tag{14}$$

Equation (13) is adequate for determining the initial stiffness of uncracked URM walls when subjected to low levels of lateral force, but URM is not a homogeneous material, and moreover there is some cracking before the effective yield point is reached. As such, modifications to the input parameters are necessary in order to satisfactorily determine the initial stiffness before effective yield. It is suggested that I_{eff} should be taken as a proportion of I_g, and similarly G_{eff} is suggested to be taken as a fraction of the uncracked shear stiffness G_m. ASCE/SEI 41-06 (2007) suggests that for determining the effective stiffness of reinforced concrete walls and reinforced masonry walls, in terms of flexural rigidity, the cracked section stiffness should be taken as equal to $0.5I_g$. For URM walls, little guidance is given on what proportion of I_g is appropriate to use to determine the cracked section stiffness. Furthermore, ASCE/SEI 41-06 (2007) states that "the shear stiffness of post-cracked masonry should be taken as a fraction of the initial uncracked masonry shear stiffness value" but no specific value is given.

Drift Capacity

Magenes and Calvi (1997) state that when sliding occurs along a single continuous bed-joint, there is no practical displacement or drift limit for the wall itself, although NZSEE (2006) suggests a drift (θ) limit of 1.0% to protect non-structural components. If sliding occurs in a stair-stepped failure pattern it is reasonable to expect that there will be a limiting displacement beyond which the wall will lose the capacity to support gravity loads, and the difference between these failure modes should be highlighted. The drift

Journal of Structural Engineering. Submitted April 12, 2011; accepted May 3, 2013;
posted ahead of print May 6, 2013. doi:10.1061/(ASCE)ST.1943-541X.0000863

which corresponds to loss of gravity support for walls responding in stair stepped bed-joint sliding is usually greater than the drift corresponding to the point at which the lateral force resisting capacity is lost, and this drift is postulated in this study to be equal to the drift corresponding to half a brick length (usually equal to a brick width) if there is no significant out of plane movement at the crack. For typical New Zealand clay bricks, this displacement corresponds to 120 mm. When a section of wall on one side of a stair-stepped crack displaces more than half a brick length, that section of wall will suddenly displace vertically by a distance equal to the height of one brick course, and the wall can be considered to have lost gravity load carrying capacity (see Figure 2).

FEMA 356 (2000) suggests "collapse prevention" limit state drift limits for walls failing in bed-joint sliding (with no distinction between sliding along a continuous bed-joint or sliding on multiple bed-joints in a stair stepped pattern) as 0.4%, for primary walls. This drift limit represents the deformation at which significant lateral strength degradation begins. FEMA 356 (2000) further provides criteria for constructing the general in-plane force-displacement relation of masonry walls responding in bed-joint (deformation-controlled) sliding according to Figure 1 using the initial stiffness (Equation (13), with $I_{eff} = I_g$, and $G_{eff} = G_m$), the predicted limiting strength (Equations (9) – (12)), and the value of $d = 0.4\%$, for primary walls. Recall that ASCE/SEI 41-06 (2007) considers bed-joint sliding as force-controlled, and the force-displacement response is governed by stiffness and "lower-bound shear strength" (Equation 9). As such, no drift limits are provided for this failure mode. ASCE/SEI 41-06 (2007) and FEMA 356 both suggest the following drift limits for the rocking behaviour mode: $d = 0.4h_{eff}/l_w$ and $e = 0.8h_{eff}/l_w$.

Journal of Structural Engineering. Submitted April 12, 2011; accepted May 3, 2013;
posted ahead of print May 6, 2013. doi:10.1061/(ASCE)ST.1943-541X.0000863

EXPERIMENTAL PROGRAMME

Wall Specifications

To investigate the strength models developed by Yi et al. (2008) and the deformation capacities for the failure modes described above, three walls, termed walls A6, A7 and A8, were constructed and tested with specifications as summarised in Table 2. All walls were 4000 mm long and 2000 mm high, with an aspect ratio of 1:2, and both the in-plane walls and out-of-plane flanges were two wythes thick (b_f = b_w = 230 mm), see Figure 3. The axial load on wall A6 was 73 kN, and corresponded to an axial stress (f_m) of 41 kPa. Similarly, the axial load on walls A7 and A8 was 76 kN and 71 kN, corresponding to an axial stress (f_m) of 56 kPa and 52 kPa, respectively. To investigate the influence of different flange arrangements, the walls had flanges positioned at different locations as shown in Figure 3.

Wall Construction and Test Setup

The walls were intentionally constructed in a manner that replicated the observed, often deteriorated, finished quality of walls in real New Zealand URM buildings and similar to URM buildings in many other parts of the world. The bricks used to construct the walls were vintage kiln fired clay bricks recovered from a demolished building, and had dimensions of 230 mm × 110 mm × 76 mm (length, width, height). The walls were

Journal of Structural Engineering. Submitted April 12, 2011; accepted May 3, 2013;
posted ahead of print May 6, 2013. doi:10.1061/(ASCE)ST.1943-541X.0000863

constructed with a common bond pattern (header bricks every 4th course) and with 1:2:9 mortar (cement:lime:sand, by volume), corresponding to ASTM type 'O' mortar, and with nominally 10 mm thick mortar joints. This mortar mix was selected based on relevant experimental results published in Dizhur et al. (2009). The typical wall setup is shown in Figure 4. The wall specimens were loaded laterally by means of an hydraulic actuator reacting against the laboratory strong wall. A steel channel was mortared to the top of the wall (the steel channel did not extend over the flanges), and the lateral forces were transferred through vertical plates welded to the underside of the steel channel on the outside of the wall-flange connection. The plates extended approximately 100 mm below the channel. Thus the applied horizontal force was transferred into the wall through both friction between the top surface of the wall and the underside of the steel beam and also directly through the vertical plates onto the top course of the wall. The axial load was applied through two box beams positioned near each end of the wall and straddling the steel beam on the top of the wall specimens. Axial load was applied to each box beam with external post-tensioning tendons connecting the box beams to the strong floor. The steel channel was 300 mm by 90 mm, and was assumed to be rigid in terms of distributing to applied axial forces uniformly into the top of the wall.

Instrumentation

Extensive instrumentation was installed on each of the six walls to capture all facets of wall response, with a typical layout shown in Figure 5.

Journal of Structural Engineering. Submitted April 12, 2011; accepted May 3, 2013;
posted ahead of print May 6, 2013. doi:10.1061/(ASCE)ST.1943-541X.0000863

The lateral force was recorded between the hydraulic jack and the wall through a load cell. The control displacement (DISP1) was recorded at the opposite end of the wall, between the top of the wall (at a point attached to the bricks immediately below the bottom surface of the loading beam) and an independent frame, to eliminate any effects from flexibility of the strong-wall. This displacement reading was obtained using a portal gauge with a displacement range of ±50 mm.

Test Procedure

The cyclic loading sequence adopted for all tests was that shown in Figure 6 and consisted of a series of displacement-controlled components. Each stage of loading consisted of one cycle to the selected tip displacement. This displacement-controlled pseudo-static procedure was employed to capture the non-uniformly accumulated damage in the wall, and to enable observations of damage and failure mechanisms. Each wall was subjected to displacements of 0.5 mm in each direction, then 1 mm in each direction and then the displacements were increased by increments of 1 mm each cycle until 10 mm was reached. For cycles with displacements above 10 mm, the displacements were increased by increments of 2 mm. During the first stages of testing, the potential for shear failure of the wall meant that small displacement increments were necessary in order to avoid the wall being loaded to failure at an early stage of testing. The push direction was defined as positive and the pull direction as negative.

Experimental Results

Journal of Structural Engineering. Submitted April 12, 2011; accepted May 3, 2013;
posted ahead of print May 6, 2013. doi:10.1061/(ASCE)ST.1943-541X.0000863

General results are presented in Table 3, where d_{80} and θ_{80} are the lateral wall displacement and drift, respectively, corresponding to the point at which the lateral force had degraded to $0.8V_u$ (see Figure 7). Tomaževič (1996) suggested that $V_u = 0.9V_{max}$ is appropriate for energy equivalence in masonry walls failing in shear, and as such $0.8V_u = 0.72V_{max}$. In Table 3 – Table 5, $A7_c$ refers to Wall A7 when the flange was in compression, and $A7_t$ refers to Wall A7 when the flange was in tension.

All walls were observed to experience diagonal tension failure with stair-stepped cracking through mortar joints, followed by sliding along the cracked bed-joints. For each wall, cracking initiated in the top course of the web, and the crack propagated downwards at an angle greater than 45°. Cracking was also evident in the flanges. For the non-symmetrical wall, A7, cracking in both directions initiated in the top course and the angle of propagation down to the bottom of the wall was steeper than 45° in the positive displacement direction (flange in compression). In the negative displacement direction (flange in tension), cracking also occurred in the compression toe, and the cracks in the web formed at approximately 45°. Figure 8 shows the final cracking patterns of each wall.

Force-Displacement Response

The force-displacement response for walls A6, A7 and A8 is shown in Figure 9. It was observed that for walls with an aspect ratio of 1:2 and flanges corresponding to $4b_f$ on

Journal of Structural Engineering. Submitted April 12, 2011; accepted May 3, 2013;
posted ahead of print May 6, 2013. doi:10.1061/(ASCE)ST.1943-541X.0000863

each side of the in-plane wall, loss of lateral strength was not sudden and there was some observable strength degradation after the peak lateral force was obtained.

Wall A6 reached a drift of 0.39%, corresponding to the peak lateral force in the positive direction first, and an ultimate drift of 0.91% corresponding to $0.8V_{max}$. Similar to Wall A6, Wall A8 reached a peak lateral force at 0.18% in the positive direction first and exhibited an ultimate drift of 0.96%. See Table 3. This indicates that for an in-plane wall controlled by diagonal tension (with cracking through the mortar joints) followed by sliding, there can be some residual displacement capacity beyond the drift limit of 0.4% suggested in FEMA 356.

The response of Wall A7 was not symmetrical, as was expected due to the non-symmetrical geometry of the wall (see Figure 3). The ultimate drift capacity in the push direction (flange in compression) was 0.63% and in the pull direction (flange in tension) was 0.74%. Overall, fat hysteretic loops were evident in both directions, and the energy dissipation characteristics are outlined below. Post-peak strength degradation was observed more in the pull (negative) direction than in the push (positive) direction.

Energy Dissipation

From the hysteretic response shown in Figure 9 the equivalent viscous damping ratio of Walls A6, A7 and A8 were obtained, and are shown in Figure 10. From the results of these tests, consistently large equivalent viscous energy damping ratios were evident, and

Journal of Structural Engineering. Submitted April 12, 2011; accepted May 3, 2013;
posted ahead of print May 6, 2013. doi:10.1061/(ASCE)ST.1943-541X.0000863

an average lower bound value of ξ_{eq} = 0.15 is suggested for flanged walls responding in a diagonal tension failure. Experimentation reported on similar walls without flanges showed an upper bound value of ξ_{eq} = 0.16 (Magenes and Calvi, 1997). These results indicate that the capacity of flanged walls to dissipate energy is greater than walls without flanges.

Crack Pattern Analysis

Conceptualised sketches of the cracking patterns of Walls A4 – A7 are shown in Figure 8. The length of the flange l_f as shown in Figure 11 refers to the total flange length. The actual cracking patterns are shown in Figure 8.

An explanation as to why there are different crack patterns associated with walls having different flange characteristics can be made by comparing the properties of flanged URM walls with the properties of thin-walled channel sections (typically steel beams). As shear force V is applied parallel to the web of a thin-walled section, which in this case is analogous to the in-plane wall, the distribution of shear stresses τ can be obtained from Equation (15) (Gere and Timoshenko, 1997).

$$\tau_{web} = \frac{V}{b_w I}\int_{A'} y dA' \tag{15}$$

When no flanges are present the shear stress varies parabolically from $\tau = 0$ at the ends of the web where $y = \pm l_w/2$, to a maximum of $\tau_{max} = 3V/2l_w b_w$ at the centre of the web. The ratio of maximum shear stress to the shear stress at the ends of the web is infinity. When

Journal of Structural Engineering. Submitted April 12, 2011; accepted May 3, 2013;
posted ahead of print May 6, 2013. doi:10.1061/(ASCE)ST.1943-541X.0000863

flanges are present, the distribution of shear stress in the flanges can be obtained from Equation (16) (Gere and Timoshenko, 1997),

$$\tau_{flange} = \frac{Vxl_w}{2I} \tag{16}$$

and the shear stress varies with x linearly along the length of the flange from $\tau = 0$ at the ends of the flange where $x = 0$, to a maximum of $Vl_f/2I$ at the web-flange junction where $x = l_f$ (for a flange on one side). For continuity of shear flow, the shear stress at the end of the web is equal to the maximum shear stress in the flange. Assuming that the thickness of the flange and the thickness of the web are equal, the ratio of the maximum shear stress at the centre of the web to the maximum shear stress at the web-flange junction can be obtained from Equation (17).

$$\frac{\tau_{flange}}{\tau_{flange,\max}} = 1 + \frac{l_w}{4l_f} \tag{17}$$

For a constant l_w, the shear stress at the ends of the in-plane wall increases with increasing flange length, relative to the maximum shear stress at the centre of the wall. Then, for a constant tensile cracking strength of masonry f_{dt}, the angle of cracking increases with increasing shear stress. This increase is because the angle between the direction of maximum principal tension stress and the state of pure stress decreases as the maximum shear stress increases (see Figure 12, where σ_1, σ_2 and τ are the maximum principal (tension) stress, the minimum principal (compression) stress and shear stress, respectively). Consequently, walls with longer flanges will develop steeper diagonal tension cracks near the ends of the in-plane wall when compared with walls with shorter flanges (see Figure 11). This effect lessens with increasing flange length, and when the flange is longer than the effective length ($6b_f$), the difference in crack angle is negligible.

Journal of Structural Engineering. Submitted April 12, 2011; accepted May 3, 2013;
posted ahead of print May 6, 2013. doi:10.1061/(ASCE)ST.1943-541X.0000863

COMPARISON OF TEST RESULTS WITH PREDICTIVE MODELS

The following sections compare the measured response of the flanged wall specimens with the predictive models described previously for stiffness, strength and drift capacity.

Initial Stiffness

The measured initial stiffness (K_{im}) was determined as the secant stiffness at $0.75V_u$ (see Figure 4). To determine the effective shear area, an effective wall thickness and length must be assumed. For two-wythe walls, $b_{w,eff}$, the effective wall thickness, should be taken as $5/8b_w$ because the collar joint between wythes is typically not completely filled, although some connection can be reasonably assumed due to the header bricks being located at every 4th course (over 4 courses, the average b_w is $0.5b_w \times 3 + 1.0b_w = 5/8b_w$). The effective wall length, $l_{w,eff}$, is taken as the clear length between flanges, determined from Equation (18) when flanges are present at both ends of the wall, and from Equation (19) when the flange is located at one end only.

$$l_{w,eff} = l_w - 2b_f \tag{18}$$

$$l_{w,eff} = l_w - b_f \tag{19}$$

Using Equation (13) and assuming $I_{eff} = 0.5I_g$ and $G_{eff} = 0.2G_m$, the average ratio of measured to calculated stiffness, K_{im}/K_{ic}, for Walls A6 – A8 considering loading in both directions was 1.02 (as shown in Table 4). The coefficient of variation for the ratio of K_{im}/K_{ic} for this data set is 21%, and as such further experimentation would be necessary to refine this approximation.

Journal of Structural Engineering. Submitted April 12, 2011; accepted May 3, 2013;
posted ahead of print May 6, 2013. doi:10.1061/(ASCE)ST.1943-541X.0000863

Predicted Strengths of Test Walls A6 – A8

Equations 1 – 12 were used to determine the predicted lateral strength of each of the test walls reported in this article. Walls A6 and A8 were symmetrical walls with flanges at both ends, with $a_i = l_w/2$, and $a_f = 2a_i$, such that $a_f = l_w$ for the Yi et al. models (Equations 1-4). For Wall A7 in the push cycle (positive displacement direction) the flange was in compression and $a_f = 0$, $a_i = l_w/3$. When the flange is at the toe of the wall (i.e. the flange is in compression) the flange reduces the compressive stress at the toe, and tends to increase the flexural strength (rocking/toe crushing), but does not tend to increase the diagonal tension strength. For Wall A7 in the pull cycle (negative displacement direction) the flange was in tension and $a_f = l_w$, $a_i = 2l_w/3$. In this case the diagonal tension strength was increased due to the weight of the tension flange. The models developed by Yi et al. (2008) predicted that diagonal tension V_{dt} (Equation 3) would be the failure mode for Walls A6 – A8. Equation (3) does not differentiate between diagonal tension with cracking through the units and diagonal tension with cracking through the mortar bed-joints. As stated above, this failure mode occurs when the principal tension stress σ_1 exceeds the diagonal tension strength of the masonry f_{dt}, which is controlled by the weaker of the mortar joint strength and the brick strength. For the test specimens, and similar to many existing conditions in URM buildings, the mortar joints were weaker than the bricks.

Journal of Structural Engineering. Submitted April 12, 2011; accepted May 3, 2013;
posted ahead of print May 6, 2013. doi:10.1061/(ASCE)ST.1943-541X.0000863

As noted previously, Tomaževič (1996) suggested that $V_u = 0.9V_{max}$ is an appropriate approximation to maintain equivalent energy in the hysteretic response for URM walls failing in shear. It is recommended here that the Yi et al (2008) model for diagonal tension (Equation (3)) also be modified by a coefficient of 0.9.

$$V_{dt} = 0.9V_{dt\ Eqn\ 3} \tag{20}$$

This empirically determined strength-reduction coefficient produces a better agreement than the original form of Equation (3). Table 5shows the comparison between the predicted maximum strength and measured maximum strength, using both Equation (20) and the expressions available in the NZSEE guidelines (2006) and ASCE/SEI 41-06 (2007), which were developed for in-plane loaded piers neglecting flanges. Using Equation (20), the average ratio of V_{max}/V_n was 1.05, with a COV of 6.7%, indicating a high level of accuracy. The NZSEE (2006) guidelines and ASCE/SEI 41-06 (2007) both predicted sliding shear as the failure mode, where no distinction was made between stair-stepped bed-joint sliding and continuous bed-joint sliding. As shown in Table 5, on average walls A6 – A8 were 29% stronger than predicted by the NZSEE (2006) guidelines and 48% stronger than predicted by ASCE/SEI 41-06 (2007), indicating the conservatism inherent in the performance assessment of in-plane loaded URM walls when neglecting the influence of flanges. Consequently, the modified Equation (3) is suggested as a more accurate estimation of the strength of flanged in-plane loaded URM walls failing in diagonal tension through the mortar joints, followed by sliding shear.

Comparison of Wall Strength with and without Flanges

Journal of Structural Engineering. Submitted April 12, 2011; accepted May 3, 2013;
posted ahead of print May 6, 2013. doi:10.1061/(ASCE)ST.1943-541X.0000863

A further wall, termed wall A4, with the same web dimensions and aspect ratio as walls A6 – A8 but with no flanges, was also tested in an identical experimental regime. This test was not continued to a limiting displacement such that direct comparison of drift capacity with walls A6 – A8 was not possible, but comparisons of strength and the effects of flanges are instructive. The maximum strength attained in both the positive and negative displacement directions of wall A4 was 62.6 kN. The maximum strength attained by the walls with flanges was 75 kN, and occurred in wall A7 with a flange in tension only and no flange in compression ($A7_t$). The lowest maximum strength attained by the walls with flanges was 61.9 kN, and also occurred in wall A7 with a flange in compression only and no tension flange ($A7_c$). This behaviour indicates that a tension flange has the effect of increasing the lateral strength, whilst the comparison between the maximum strength of wall A4 and wall $A7_c$ suggests that a compression flange (and lack of a tension flange) does not increase the lateral strength. The maximum strengths of walls A6 and A8 were approximately equal to the average of the maximum strengths of wall A7 (68.5 kN). This comparison suggests that whilst a tension flange increases the wall lateral strength, a compression flange acting at the same time can reduce the effect of the tension flange. Moon et al. (2006) noted that global and component tension flanges affect the response of URM walls by providing additional weight, and also that compression flanges have a negligible effect on the bed-joint sliding and diagonal tension strength. This observation shows a reasonable correlation with the experimental results of walls A6 – A8, and the comparison with wall A4.

Journal of Structural Engineering. Submitted April 12, 2011; accepted May 3, 2013;
posted ahead of print May 6, 2013. doi:10.1061/(ASCE)ST.1943-541X.0000863

Additional experimentation or parametric numerical modelling would be necessary to further clarify the effects of flanges on lateral strength and failure modes.

Drift Capacity

All the walls reported failed by diagonal tension cracking with cracks through the mortar joints, followed by stair-stepped bed-joint sliding. The values of θ_{80} in both push and pull directions for Walls A6 – A8 for all flange configurations is shown in Table 3. Note that the drift reported herein is the wall displacement normalised by the wall height, 2 m for wall specimens.

For comparison, Magenes and Calvi (1997) reported ten values of θ_{80} from in-plane quasi-static cyclic tests on unreinforced masonry piers without flanges. From these tests the mean value of drift θ_{80} was 0.53%, with a COV of 11%, and the maximum and minimum values were 0.62% and 0.44% respectively. As the minimum value of θ_{80} for walls A6 – A8 with flanges was greater than the maximum value for walls without flanges reported by Magenes and Calvi (1997), it appears that one effect of flanges is to increase the deformation and drift capacity of in-plane loaded URM walls. Similarly, the drifts attained by Walls A6 – A8 were greater than 0.4% as proposed in FEMA 356 for bed joint sliding. ASCE/SEI 41-06 (2007) considers the wall specimens as "force-controlled" and hence do not allow for any drift capacity beyond the drift at V_{bjs} from Equation 9.

Journal of Structural Engineering. Submitted April 12, 2011; accepted May 3, 2013;
posted ahead of print May 6, 2013. doi:10.1061/(ASCE)ST.1943-541X.0000863

The mean value of drift capacity for Walls A6 and A8 was 0.96%. In each imposed displacement direction for these two wall specimens there was a flange supporting the compression end of the web. The value of drift capacity for Wall A7 when the flange was in compression was 0.74%, and was greater than the corresponding value (0.63%) when the flange was in tension (no compression flange). This observation suggests that the drift at loss of lateral load capacity is less if there is no flange supporting the compression end of the web. This result is consistent with the findings of Magenes and Calvi (1997) where flange effects are not accounted for.

Based on the above discussion and the results for walls A6-A8, it is suggested that for walls with compression flanges the drift capacity at loss of lateral load capacity can be estimated as 0.7%. Considering the limited size of the data set available, this recommendation is taken as equal to the minimum drift achieved by any of the wall specimens with a flange supporting the compression end of the web. This drift limit could be modified if a larger data set is available in the future. It should be noted that this suggested drift limit is based on the results of one test only and further experimentation should be undertaken. Moreover, the interaction between flanges acting in tension and a flange acting in compression warrants further investigation. For walls without a flange supporting the compression end of the web, the drift capacity at loss of lateral load capacity can be estimated as 0.4%, selected to be consistent with FEMA 356 and Magenes and Calvi (1997) recommendations for walls without flanges.

Journal of Structural Engineering. Submitted April 12, 2011; accepted May 3, 2013;
posted ahead of print May 6, 2013. doi:10.1061/(ASCE)ST.1943-541X.0000863

Further experimentation would be necessary for estimating strength and drift limits corresponding to different modes of failure.

Due to actuator stroke limitations, Walls A6 – A8 were not taken to the point of axial load failure. Considering the stair-stepped crack, it may be reasonably suggested however that axial load failure will occur at half a brick length or 120 mm.

GENERAL FORCE-DISPLACEMENT RESPONSE OF URM WALLS WITH FLANGES

The measured hysteretic response and predicted response of Walls A6 – A8 are shown in Figure 9. A proposed backbone model is also included in the figures with stiffness determined from Equation 13 with $I_{eff} = 0.5I_g$ and $G_{eff} = 0.2G_m$, strength determined from Equation 20, and using a drift at lateral failure-load of 0.7% and drift at axial failure-load (drift *e* from Figure 1) corresponding to half a brick length (120 mm). For clarity, the scale of the figure does not continue to drift *e*.

The general in-plane relation of masonry walls responding in bed-joint sliding according to FEMA 356 is also shown in Figure 9. The initial stiffness from the FEMA 356 backbone assumes $I = I_g$ and $G = G_m$, and as such is higher than that proposed in the model, and observed in the test data. Similarly the maximum force attained according to the FEMA 356 is lower than that predicted by the modified Equation (3), where flanges are accounted for. The drift corresponding to loss of lateral force resistance is assumed

Journal of Structural Engineering. Submitted April 12, 2011; accepted May 3, 2013;
posted ahead of print May 6, 2013. doi:10.1061/(ASCE)ST.1943-541X.0000863

as 0.4% in FEMA 356, but 0.7% in the proposed model, except in wall $A7_t$ where this drift is taken as 0.4% (see Figure 9(b)), because there is no flange in compression. Finally the drift corresponding to loss of gravity support is assumed as 0.8% in FEMA 356 (indicated by a solid bullet in Figure 9), which appears to be conservative for diagonal tension failures through the mortar joints.

Recall that ASCE/SEI 41-06 (2007) adopts a very conservative assessment and considers all three walls as force-controlled and predicts failure at the "yield displacement" shown for the FEMA 356 backbone.

CONCLUSIONS

Flanged walls A6 – A8, subjected to reversed cyclic in-plane shear, failed by diagonal tension cracking through the mortar joints, and subsequently commenced sliding on the bed-joints. Flanges on the compression end of the walls resulted in an increase in drift capacity. The lowest value of θ_{80} from the results of testing Walls A6 – A8 with a flange in compression was 0.74%. Thus for walls with compression flanges failing in a diagonal tension mode followed by bed-joint sliding, a drift limit at lateral load failure of 0.7% is suggested from this limited data set.

A modified version of the diagonal tension shear strength model by Yi et al. (2008), with a pre-multiplier coefficient of 0.9, was validated using the experimental results of

Journal of Structural Engineering. Submitted April 12, 2011; accepted May 3, 2013;
posted ahead of print May 6, 2013. doi:10.1061/(ASCE)ST.1943-541X.0000863

walls A6 – A8, with a high level of correlation, and is suggested for predicting the diagonal tension strength of flanged URM walls.

The initial stiffness of URM walls failing in diagonal tension followed by bed-joint sliding was satisfactorily modelled using Equation (5), with modifications made to the shear modulus and effective moment of inertia, to account for cracking and the non-homogeneous nature of masonry. The effective shear stiffness, G_{eff}, is suggested to be taken as $0.2G_m$, and I_{eff} is suggested to be taken as $0.5I_g$.

Determining the initial stiffness, strength and drift capacity of URM walls experiencing diagonal tension cracking followed by bed-joint sliding enabled the general force-displacement response to be modelled, as per Figure 1, producing reasonable agreement with the measured hysteretic behavior.

The effect of flanges is significant and increases the displacement capacity of in-plane loaded walls when the flange is in compression, compared to similar walls without flanges. Moreover, a flange acting in tension increases the lateral strength of in-plane loaded walls.

This article presented the results of flanged URM walls failing by diagonal tension cracking through the mortar joints, followed by sliding on the bed-joints. Further experimentation would be necessary for estimating strength and drift limits corresponding to different modes of failure.

Journal of Structural Engineering. Submitted April 12, 2011; accepted May 3, 2013;
posted ahead of print May 6, 2013. doi:10.1061/(ASCE)ST.1943-541X.0000863

NOTATION

a_i Distance between inertia centre and compression edge of wall

a_f Distance between centre of flange and compression edge of wall

A_n Area of net mortared section

A_f Cross-sectional area of flange

A_v Shear area of wall

b_f Width of flange

b_w Width of wall (web)

$b_{w,eff}$ Effective width of wall (web)

c Cohesion

COV Coefficient of variation

$d_{V,max}$ Wall displacement at V_{max}

E_m Masonry Young's modulus

f_{bt} Direct tensile strength of bricks

f_{dt} Diagonal tension strength of masonry

f_m Axial compressive stress

f'_m Compressive strength of masonry

G Shear modulus

G_m Masonry shear modulus

G_{eff} Effective post-cracked shear modulus

h_w Height of wall

h_{eff} Effective height of wall

I Moment of inertia

I_g Gross moment of inertia

I_{eff} Effective moment of inertia

K_{ic} Calculated initial stiffness

K_{im} Measured initial stiffness

Journal of Structural Engineering. Submitted April 12, 2011; accepted May 3, 2013;
posted ahead of print May 6, 2013. doi:10.1061/(ASCE)ST.1943-541X.0000863

l_f Length of flange

l_w Length of wall

$l_{w,eff}$ Effective length of wall

N Normal force on cross section

V Applied lateral force

V_b Shear strength corresponding to diagonal tension failure involving cracking through bricks

V_{bjs} Shear strength corresponding to bed joint sliding

V_{crack} Base shear at first crack

V_{dt} Shear strength corresponding to diagonal tension failure

V_j Shear strength corresponding to diagonal tension failure involving damage in mortar joints

V_{max} Maximum base shear

v_{me} Cohesive strength of masonry bed joint

V_n Predicted lateral strength

V_r Shear strength corresponding to onset of rocking

V_s Shear strength corresponding to sliding

V_{tc} Shear strength corresponding to toe crushing

V_u Equivalent ultimate base shear

W_f Weight of flange

W_w Weight of in-plane wall (web)

z Distance from extreme compression fibre to line of action of normal force (N)

α Factor equal to 0.5 for wall fixed at base and free at top

α_c Effective aspect ratio

β Factor to account for non-linear vertical stress distribution

θ Drift

θ_{crack} Wall drift at cracking

θ_{80} Wall drift corresponding to $0.8V_u$

$\theta_{V,max}$ Wall drift at V_{max}

μ Coefficient of friction

Journal of Structural Engineering. Submitted April 12, 2011; accepted May 3, 2013;
posted ahead of print May 6, 2013. doi:10.1061/(ASCE)ST.1943-541X.0000863

σ_1 Maximum principal stress

ζ Factor to account for wall aspect ratio

ξ Equivalent viscous damping ratio

Journal of Structural Engineering. Submitted April 12, 2011; accepted May 3, 2013;
posted ahead of print May 6, 2013. doi:10.1061/(ASCE)ST.1943-541X.0000863

REFERENCES

Abrams, D. P. (1997). "Response of unreinforced masonry buildings." *Journal of Earthquake Engineering*, 1(1), 257-273.

ASCE/SEI. (2007). *Seismic Rehabilitation of Existing Buildings - ASCE/SEI 41-06*, American Society of Civil Engineers, Reston, Va.

Atkinson, R. H., Amadei, B. P., Saeb, S., and Sture, S. (1989). "``Response of Masonry Bed Joints in Direct Shear"." *Journal of Structural Engineering*, 115(9), 2276 -- 2296.

Benedetti, D., and Tomaževič, M. (1984). "Sulla verifica sismica di costruzioni in muratura (on the seismic assessment of masonry structures)." *Ingegneria Sismica*, 1(0), 9-16. [in Italian].

Costley, A. C. (1996). *Dynamic Response of Unreinforced Masonry Buildings with Flexible Diaphragms*, University of Buffalo, Buffalo, NY, (PB97-133573, MF-A03, A15).

Derakhshan, H., Dizhur, D., Lumantarna, R., Cuthbert, J., Griffith, M. C., and Ingham, J. M. (2010). "In-Field Simulated Seismic Testing of As-Built and Retrofitted Unreinforced Masonry Partition Walls of The William Weir House in Wellington." *Journal of the Structural Engineering Society New Zealand*, 23(1), 51 - 61.

Dizhur, D., Derakhshan, H., Ingham, J. M., and Griffith, M. C. (2009). "In-Situ Out-Of-Plane Testing of Unreinforced Masonry Partition Walls." *11th Canadian Masonry Symposium*, Toronto, Ontario, Canada, May 31 - June 3, 2009.

Journal of Structural Engineering. Submitted April 12, 2011; accepted May 3, 2013;
posted ahead of print May 6, 2013. doi:10.1061/(ASCE)ST.1943-541X.0000863

Dizhur, D., and Ingham, J. M. (2010a). "Field testing of an earthquake-damaged unreinforced masonry building." *7th International Conference on Urban Earthquake Engineering (7CUEE) & 5th International Conference on Earthquake Engineering (5ICEE)*, Tokyo Institute of Technology, Tokyo, Japan, March 3 - 5, 2010.

Dizhur, D., Ismail, N., Knox, C., Lumantarna, R., and Ingham, J. M. (2010b). "Performance of Unreinforced and Retrofitted Masonry Buildings During the 2010 Darfield Earthquake." *Bulletin of the New Zealand Society for Earthquake Engineering*, 43(4), 321-339.

Dizhur, D., Ingham, J. M., Moon, L. M., Griffith, M., Schultz, A. E., Senaldi, I., Magenes, G., Dickie, J., Lissel, S., Centeno, J., Ventura, C., Leite, J., and Lourenco, P. B. (2011). "Performance of Masonry Buildings and Churches in the 22 February 2011 Christchurch Earthquake." *Bulletin of the New Zealand Society for Earthquake Engineering*, 44(4), 279-296.

FEMA 273. (1997). *NEHRP Guidelines for the Seismic Rehabilitation of Buildings*, Federal Emergency Management Agency, Washington, DC.

FEMA 356. (2000). *Prestandard and Commentary for the Seismic Rehabilitation of Buildings*, Federal Emergency Management Agency, Washington, DC.

Gambarotta, L., and Lagomarsino, S. (1997a). "Damage models for the seismic response of brick masonry shear walls. Part I: The mortar joint model and its applications." *Earthquake Engineering and Structural Dynamics*, 26(4), 423-439.

Journal of Structural Engineering. Submitted April 12, 2011; accepted May 3, 2013;
posted ahead of print May 6, 2013. doi:10.1061/(ASCE)ST.1943-541X.0000863

Gambarotta, L., and Lagomarsino, S. (1997b). "Damage models for the seismic response of brick masonry shear walls. Part II: The continuum model and its applications." *Earthquake Engineering and Structural Dynamics*, 26(4), 441-462.

Gere, J. M., and Timoshenko, S. P. (1997). *Mechanics of Materials*, PWS Pub Co., Boston.

Ingham, J. M., Biggs, D. T., and Moon, L. M. (2011a). "How did unreinforced masonry buildings perform in the February 2011 Christchurch earthquake." *The Structural Engineer*, 89(6), 14-18.

Ingham, J. M., and Griffith, M. C. (2011b). "Performance of unreinforced masonry buildings during the 2010 Darfield (Christchurch, NZ) earthquake." *Australian Journal of Structural Engineering*, 11(3), 207-224.

Magenes, G., and Calvi, G. M. (1997). "In-plane seismic response of brick masonry walls." *Earthquake Engineering & Structural Dynamics*, 26(11), 1091-1112.

Moon, F. L. (2004). "Seismic Strengthening of Low-Rise Unreinforced Masonry Structures with Flexible Diaphragms," Doctoral Dissertation. Georgia Institute of Technology, Atlanta, GA, USA.

Moon, F. L., Yi, T., Leon, R. T., and Kahn, L. F. (2006). "Recommendations for Seismic Evaluation and Retrofit of Low-Rise URM Structures." *Journal of Structural Engineering*, 132(5), 663-672.

NZSEE. (2006). *Assessment and Improvement of the Structural Performance of Buildings in Earthquakes*, Recommendations of a NZSEE Study Group on Earthquake Risk Buildings. New Zealand Society for Earthquake Engineering, Wellington, New Zealand.

Journal of Structural Engineering. Submitted April 12, 2011; accepted May 3, 2013;
posted ahead of print May 6, 2013. doi:10.1061/(ASCE)ST.1943-541X.0000863

Paquette, J., and Bruneau, M. (2003). "Pseudo-dynamic testing of unreinforced masonry building with flexible diaphragm." *Journal of Structural Engineering*, 129(6), 708-716.

Russell, A. P., and Ingham, J. M. (2010). "Prevalence of New Zealand's Unreinforced Masonry Buildings." *Bulletin of the New Zealand Society for Earthquake Engineering*, 43(3), 182-201.

Steelman, J., and Abrams, D. P. (2007). "Effect of axial stress and aspect ratio on lateral strength of URM shear walls." Tenth North American Masonry Conference, The Masonry Society, St. Louis, Missouri, USA.

Tomaževič, M. (1996). "Recent Advances in Earthquake Resistant Design of Masonry Buildings." *11th World Conference on Earthquake Engineering*, Acapulco, Mexico, June 23 - 29, 1996.

Yi, T. (2004). "Experimental Investigation and Numerical Simulation of an Unreinforced Masonry Structure with Flexible Diaphragms," Doctoral Dissertation. Georgia Institute of Technology, Atlanta, GA, USA.

Yi, T., Moon, F. L., Leon, R. T., and Kahn, L. F. (2006a). "Analyses of a Two-Story Unreinforced Masonry Building." *Journal of Structural Engineering*, 132(5), 653-662.

Yi, T., Moon, F. L., Leon, R. T., and Kahn, L. F. (2006b). "Lateral Load Tests on a Two-Story Unreinforced Masonry Building." *Journal of Structural Engineering*, 132(5), 643-652.

Yi, T., Moon, F. L., Leon, R. T., and Kahn, L. F. (2008). "Flange Effects on the Nonlinear Behaviour of URM Piers." *The Masonry Society Journal*, 26(2), 31-42.

Journal of Structural Engineering. Submitted April 12, 2011; accepted May 3, 2013;
posted ahead of print May 6, 2013. doi:10.1061/(ASCE)ST.1943-541X.0000863

Table 1: Definition of URM Failure Modes

	Rocking	Toe Crushing	Bed-joint sliding (single bed-joint)	Bed-joint sliding (stair stepped*)	Diagonal tension (crack through joints)	Diagonal tension (crack through units)
FEMA 356 Yi et al.	Deformation-controlled	Force-controlled	Deformation-controlled		N/A	Force-controlled
ASCE/SEI 06	Deformation-controlled	Force-controlled	Force-controlled ("lower-bound shear strength")		N/A	N/A
NZSEE	"Flexural failure"		"Sliding shear"	N/A	"Damage in mortar joints"	"Damage in bricks"

* after diagonal tension failure with cracking through mortar joints

Journal of Structural Engineering. Submitted April 12, 2011; accepted May 3, 2013;
posted ahead of print May 6, 2013. doi:10.1061/(ASCE)ST.1943-541X.0000863

Table 2: Wall specifications

Wall	b_w mm	h_w mm	l_w mm	μ MPa	f_m/f'_m %	Flanges at		b_f mm	l_f mm
A4	230	2000	4000	0.7	0.433	-	-	-	-
A6	230	2000	4000	0.7	0.441	both ends	both sides	230	2160
A7	230	2000	4000	0.7	0.468	one end	both sides	230	2160
A8	230	2000	4000	0.7	0.576	both ends	one side	230	1200

Journal of Structural Engineering. Submitted April 12, 2011; accepted May 3, 2013;
posted ahead of print May 6, 2013. doi:10.1061/(ASCE)ST.1943-541X.0000863

Table 3: Experimental results

Wall	V_{max} kN	$d_{V,max}$ mm	$\theta_{V,max}$ %	V_{crack} kN	θ_{crack} %	d_{80} mm	θ_{80} %	Behaviour
A6 (+)	69.3	7.8	0.39	46.4	0.04	19	0.91	Diagonal tension
A6 (-)	67.4	3.9	0.20	44.6	0.04	17	0.99	
$A7_c$ (+)	61.9	7.7	0.38	34.7	0.03	15	0.74	Diagonal tension
$A7_t$ (-)	75.0	2.8	0.14	34.5	0.03	10	0.63	
A8 (+)	66.9	3.6	0.18	60.0	0.06	19.2	0.92	Diagonal tension
A8 (-)	68.5	3.8	0.19	61.2	0.06	19.2	1.01	
Mean	68.2	4.9	0.25	46.9	0.04	16.6	0.87	
COV	6%	45%	45%	25%	32%	22%	17%	

Journal of Structural Engineering. Submitted April 12, 2011; accepted May 3, 2013;
posted ahead of print May 6, 2013. doi:10.1061/(ASCE)ST.1943-541X.0000863

Table 4: Effective initial stiffness of flanged walls

Wall	K_{im}	K_{im}/K_{ic}
	kN/mm	
A6 (+)	34.2	0.95
A6 (-)	27.6	0.77
A7c (+)	29.0	0.80
A7t (-)	45.9	1.27
A8 (+)	44.3	1.23
A8 (-)	38.8	1.08
Mean	36.6	1.02
COV	21%	21%

Journal of Structural Engineering. Submitted April 12, 2011; accepted May 3, 2013;
posted ahead of print May 6, 2013. doi:10.1061/(ASCE)ST.1943-541X.0000863

Table 5: Comparison of proposed strength accounting for and neglecting flanges

		Yi et al. model		NZSEE expressions		ASCE/SEI expressions	
Wall	V_{max} kN	V_n kN	V_{max}/V_n	V_n kN	V_{max}/V_n	V_n kN	V_{max}/V_n
A6 (+)	69.3	67.9	1.02	53.0	1.31	46.0	1.51
A6 (-)	67.4	67.9	0.99	53.0	1.27	46.0	1.47
$A7_c$ (+)	61.9	53.4	1.16	53.0	1.17	46.0	1.35
$A7_t$ (-)	75.0	67.5	1.11	53.0	1.42	46.0	1.63
A8 (+)	66.9	67.5	0.99	53.0	1.26	46.0	1.45
A8 (-)	68.5	67.5	1.01	53.0	1.29	46.0	1.49
Mean			1.05		1.29		1.48
COV			6.7%		6.2%		6.2%

Journal of Structural Engineering. Submitted April 12, 2011; accepted May 3, 2013;
posted ahead of print May 6, 2013. doi:10.1061/(ASCE)ST.1943-541X.0000863

List of Figure Captions

Figure 1: Generalised force-deformation relation for masonry elements or components (adapted from Figure 7-1, ASCE/SEI 41-06 (2007))

(a) Deformation-controlled components

(b) Force controlled-components

Figure 2: Loss of gravity support after stair-stepped cracking

Figure 3: Wall plan dimensions

(a) Wall A6

(b) Wall A7

(c) Wall A8

Figure 4: Test setup

Figure 5: Instrumentation

Figure 6: Imposed cyclic displacement history

Figure 7: Equivalent bilinear approximation (adapted from Magenes and Calvi (1997))

Figure 8: Wall cracking patterns

(a) Wall A4

(b) Wall A6

Journal of Structural Engineering. Submitted April 12, 2011; accepted May 3, 2013;
posted ahead of print May 6, 2013. doi:10.1061/(ASCE)ST.1943-541X.0000863

(c) Wall A7

(d) Wall A8

Figure 9: Measured and proposed force-displacement response

(a) Wall A6

(b) Wall A7

(c) Wall A8

Figure 10: Equivalent viscous damping ratios of Wall A6, A7 and A8

Figure 11: Flange effects on the orientation of cracking of in-plane wall

(a) Wall A4 – no flanges

(b) Wall A5 – flange length = $5b_f$

(c) Wall A6 – flange length = $9b_f$

(d) Wall A7 – flange length = $9b_f$, one end only

Figure 12: Direction of principal stresses at ends of in-plane wall

(a) Principal stress directions when no flange is present

(b) Principal stress directions when long flange is present

Figure 1a

Journal of Structural Engineering. Submitted April 12, 2011; accepted May 3, 2013;
posted ahead of print May 6, 2013. doi:10.1061/(ASCE)ST.1943-541X.0000863

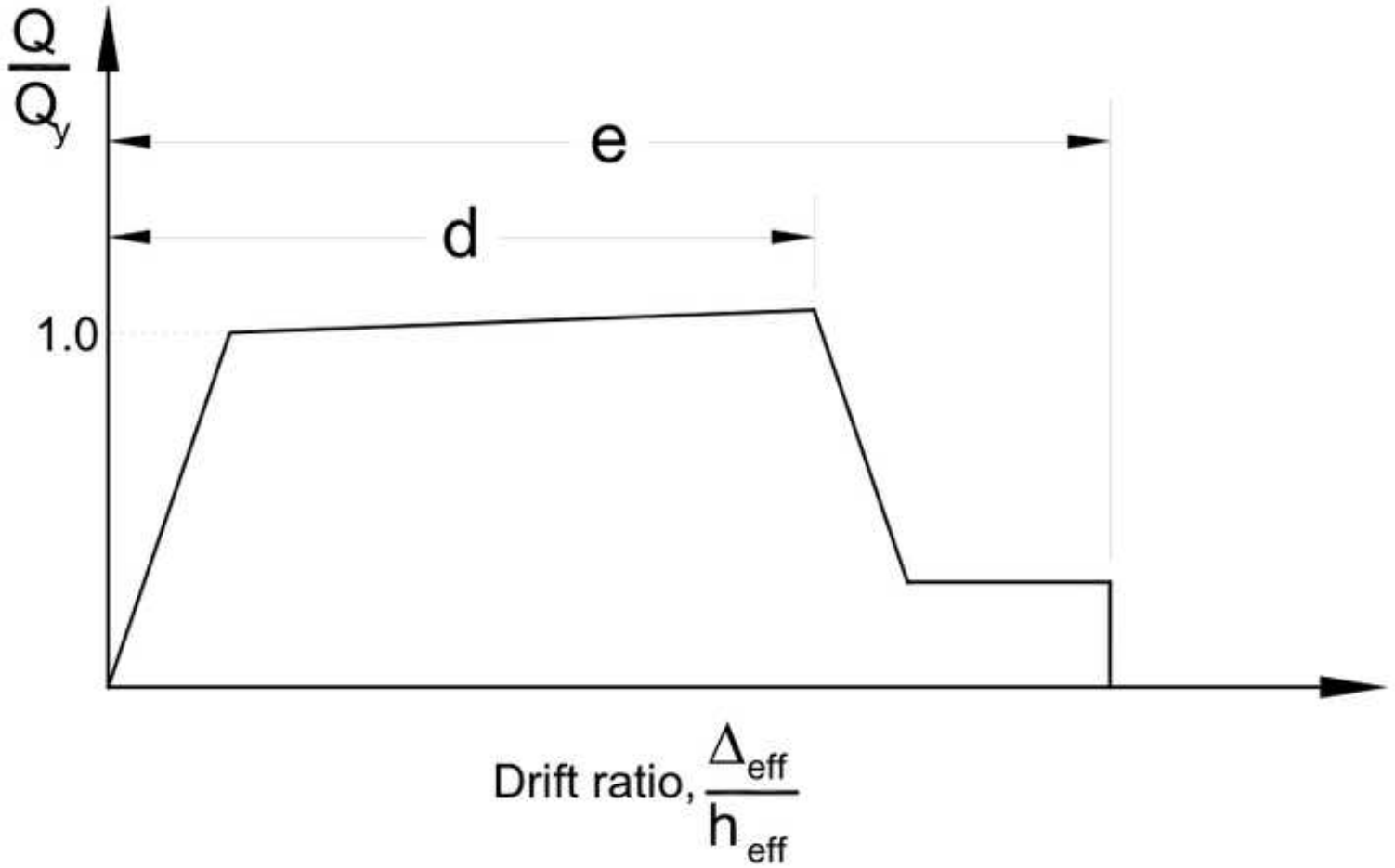

Figure 1b

Journal of Structural Engineering. Submitted April 12, 2011; accepted May 3, 2013;
posted ahead of print May 6, 2013. doi:10.1061/(ASCE)ST.1943-541X.0000863

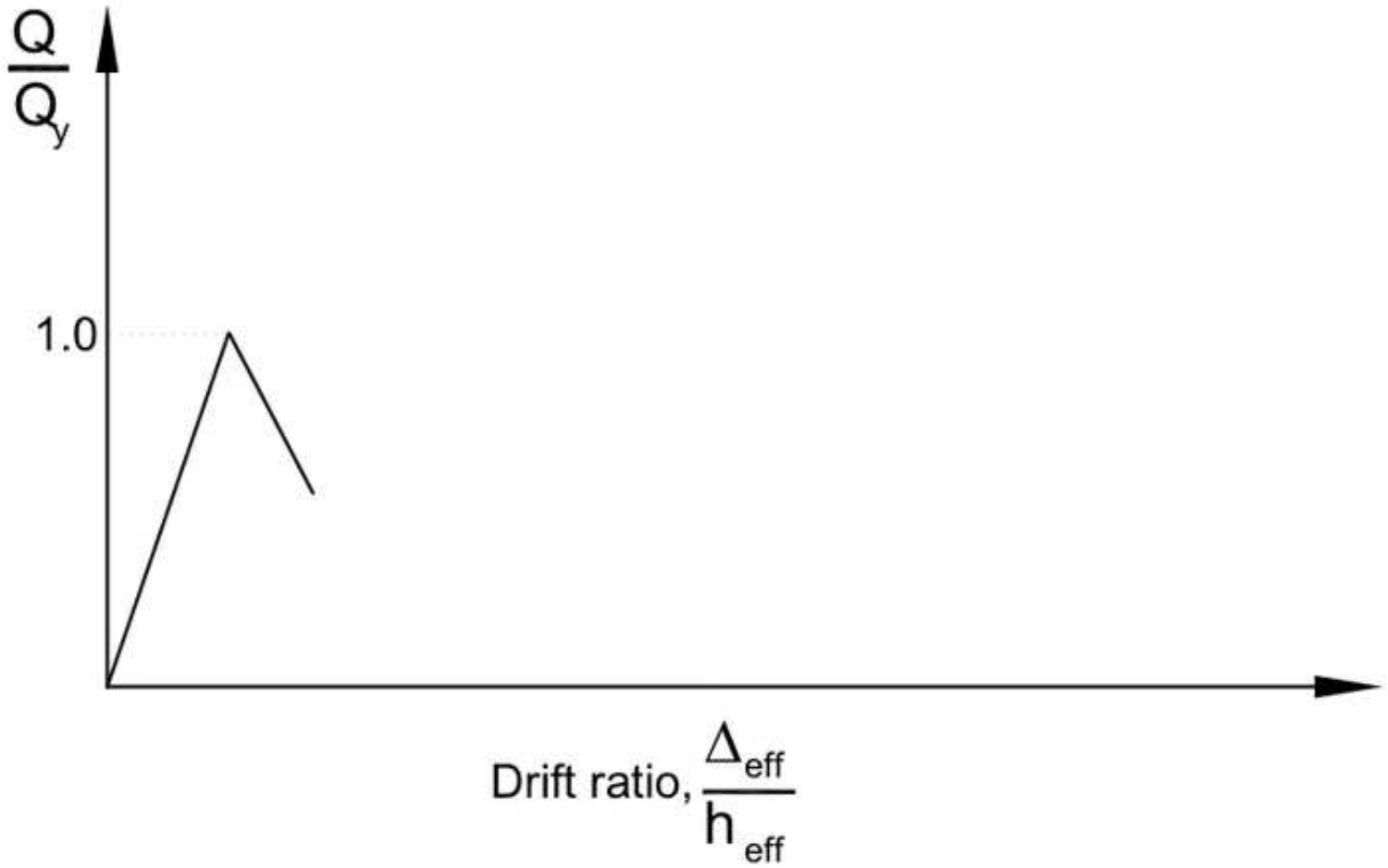

Figure 2

Journal of Structural Engineering. Submitted April 12, 2011; accepted May 3, 2013;
posted ahead of print May 6, 2013. doi:10.1061/(ASCE)ST.1943-541X.0000863

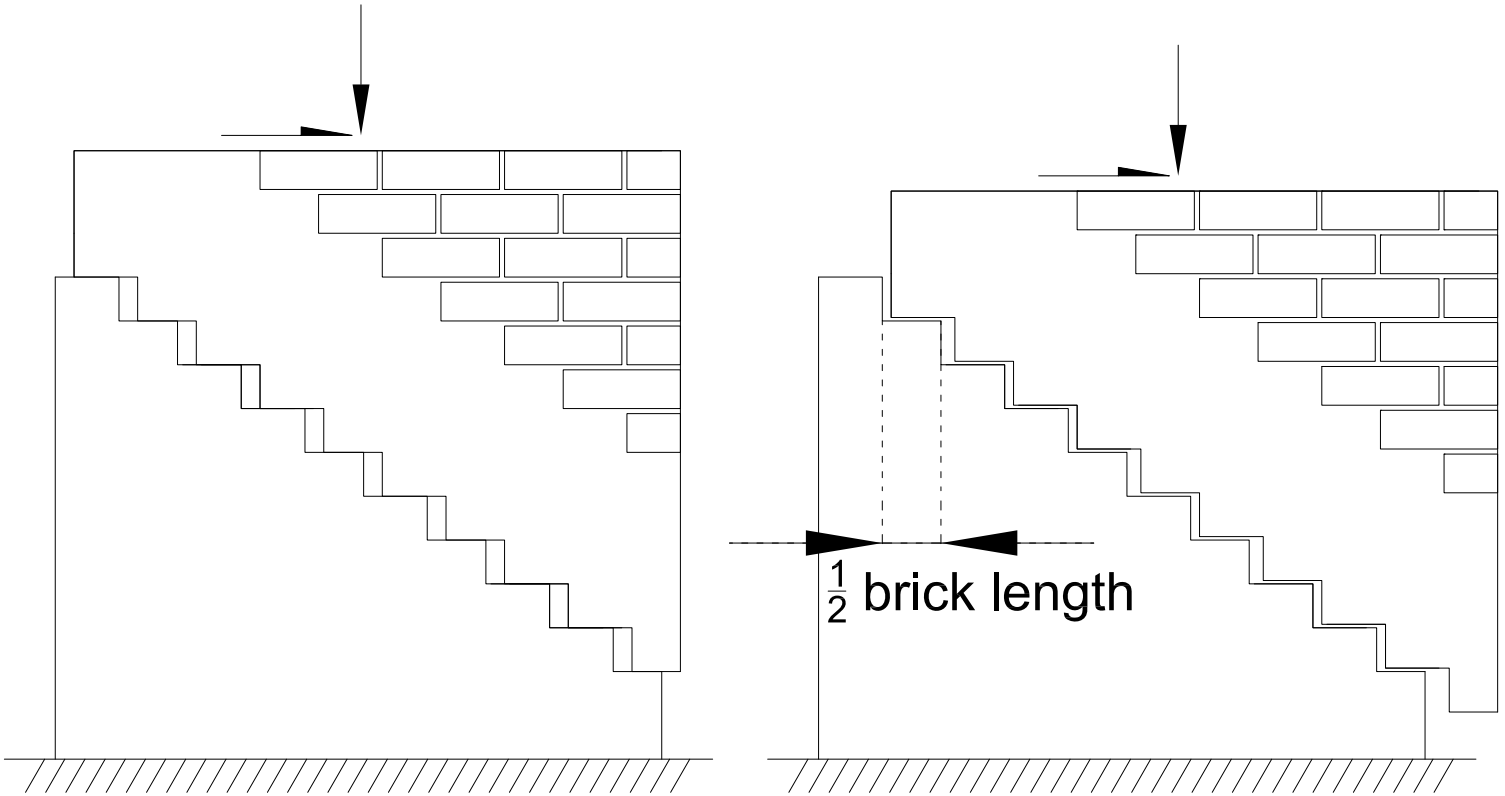

Figure 3a

Journal of Structural Engineering. Submitted April 12, 2011; accepted May 3, 2013;
posted ahead of print May 6, 2013. doi:10.1061/(ASCE)ST.1943-541X.0000863

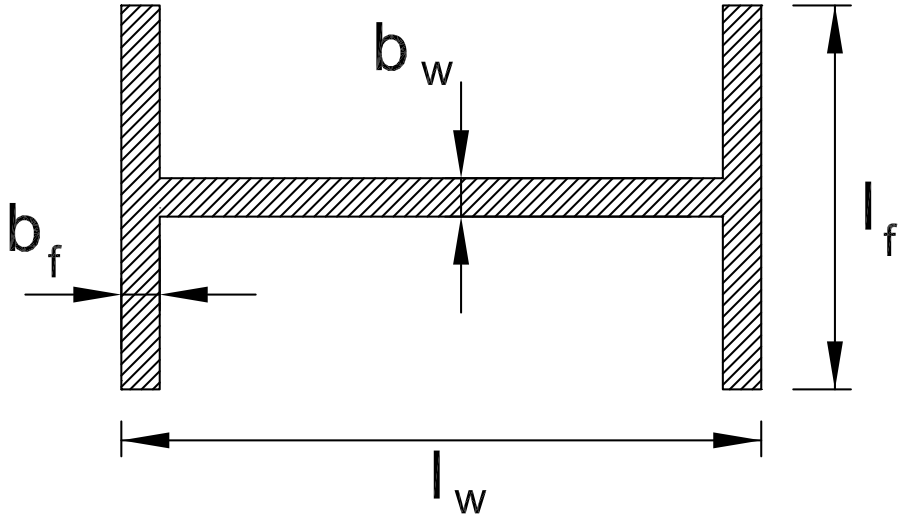

Figure 3b

Journal of Structural Engineering. Submitted April 12, 2011; accepted May 3, 2013;
posted ahead of print May 6, 2013. doi:10.1061/(ASCE)ST.1943-541X.0000863

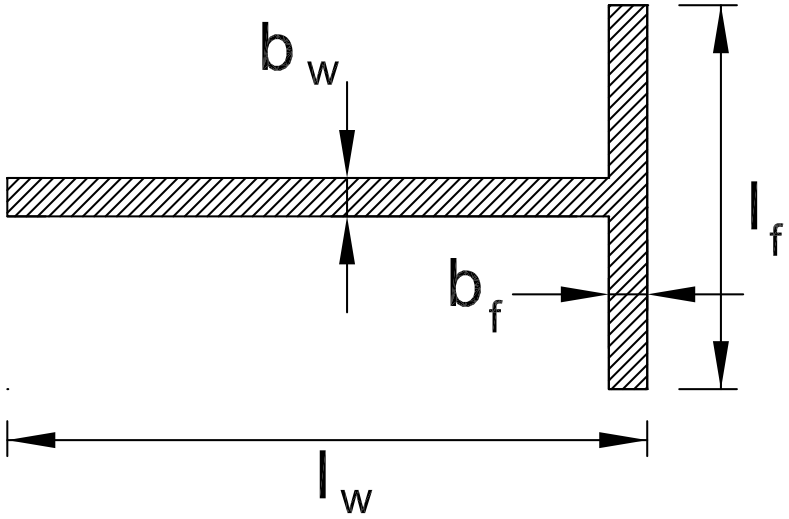

Figure 3c

Journal of Structural Engineering. Submitted April 12, 2011; accepted May 3, 2013;
posted ahead of print May 6, 2013. doi:10.1061/(ASCE)ST.1943-541X.0000863

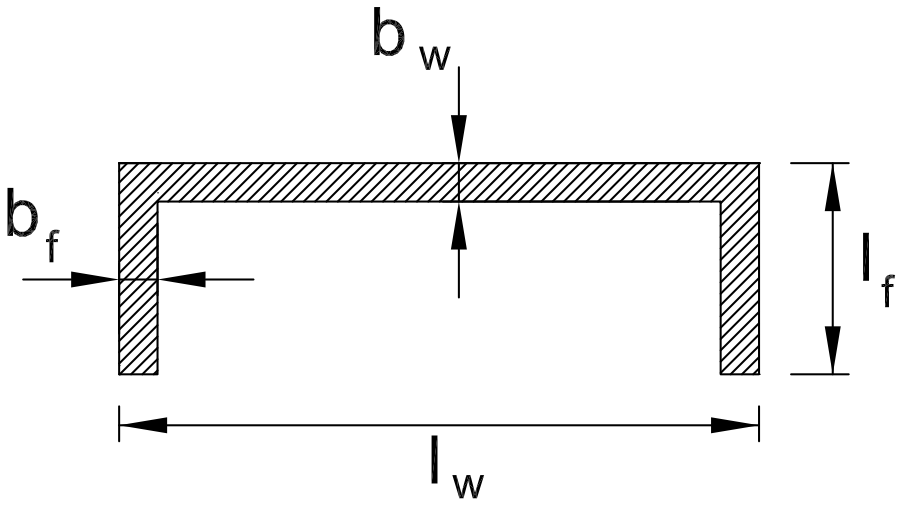

Figure 4

Journal of Structural Engineering. Submitted April 12, 2011; accepted May 3, 2013;
posted ahead of print May 6, 2013. doi:10.1061/(ASCE)ST.1943-541X.0000863

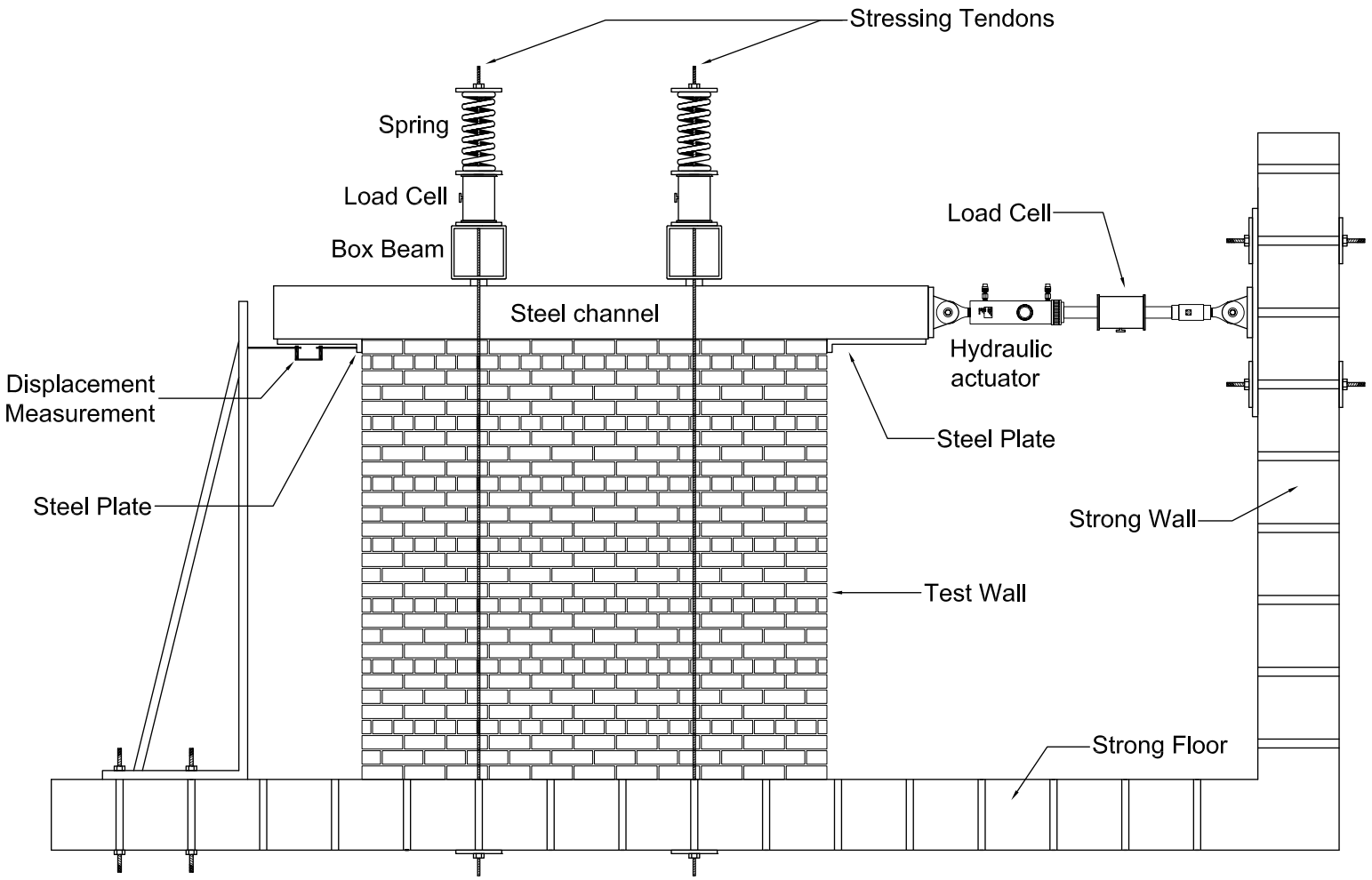

Figure 5

Journal of Structural Engineering. Submitted April 12, 2011; accepted May 3, 2013;
posted ahead of print May 6, 2013. doi:10.1061/(ASCE)ST.1943-541X.0000863

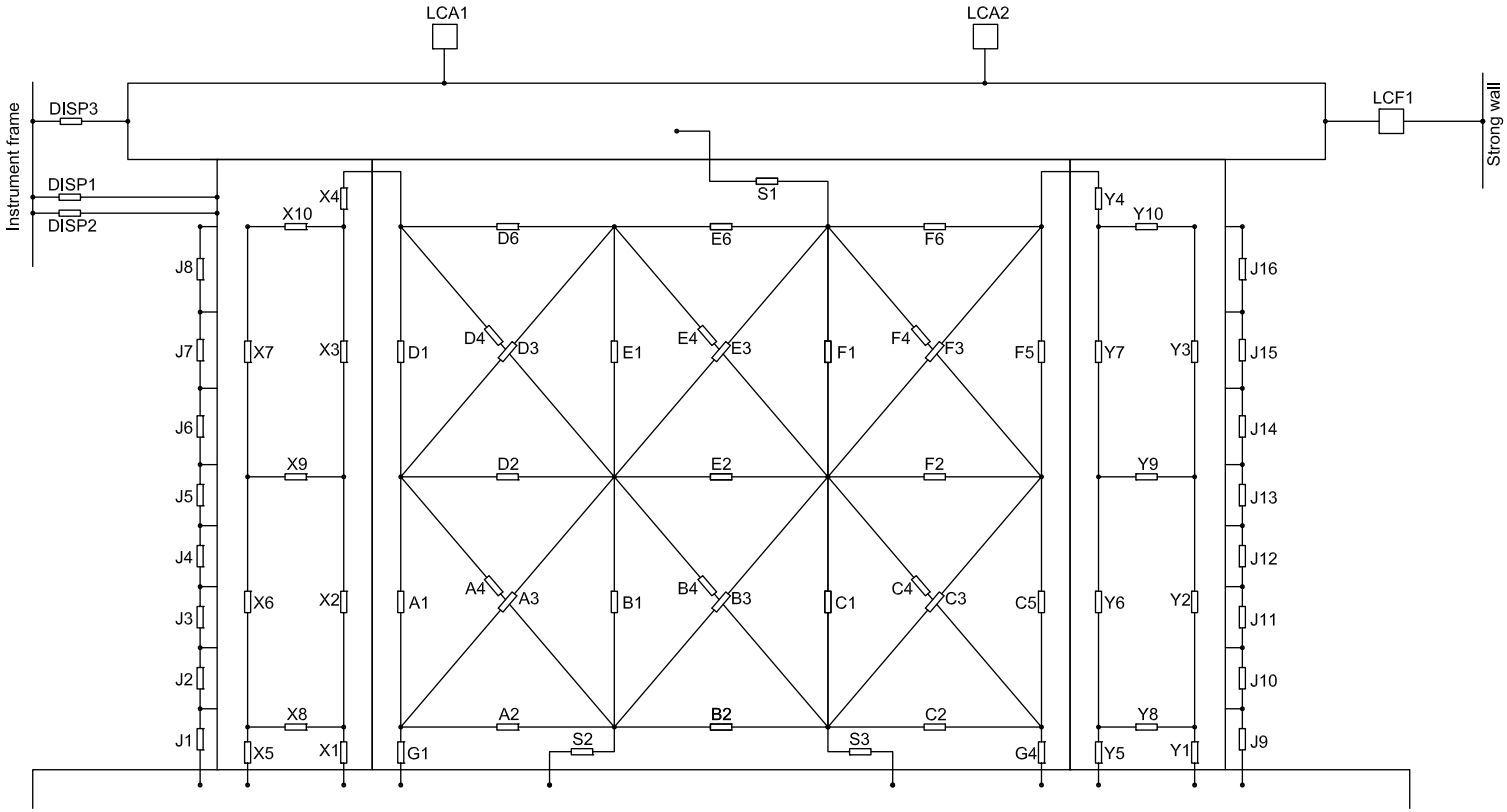

Figure 6

Journal of Structural Engineering. Submitted April 12, 2011; accepted May 3, 2013;
posted ahead of print May 6, 2013. doi:10.1061/(ASCE)ST.1943-541X.0000863

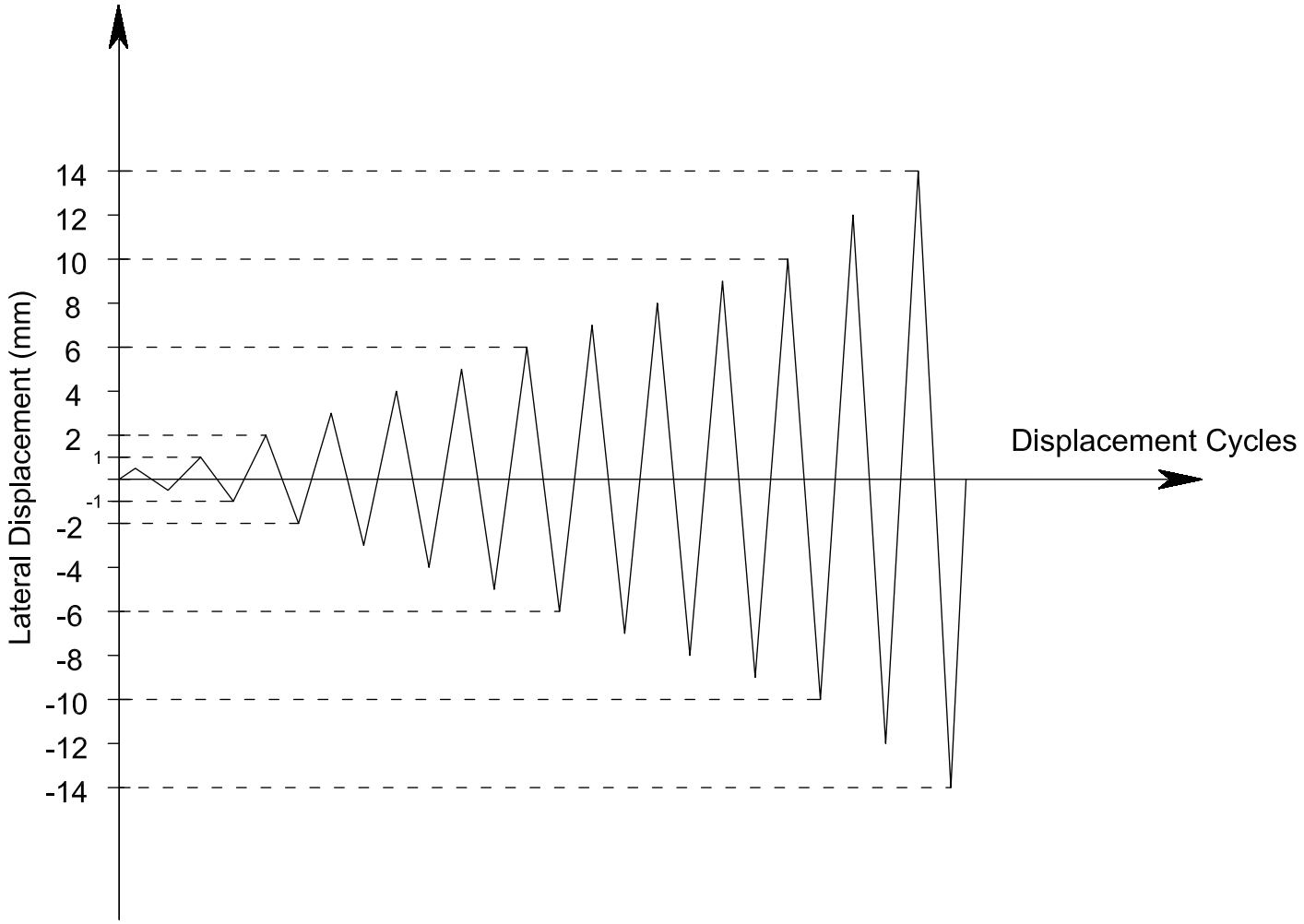

Figure 7

Journal of Structural Engineering. Submitted April 12, 2011; accepted May 3, 2013;
posted ahead of print May 6, 2013. doi:10.1061/(ASCE)ST.1943-541X.0000863

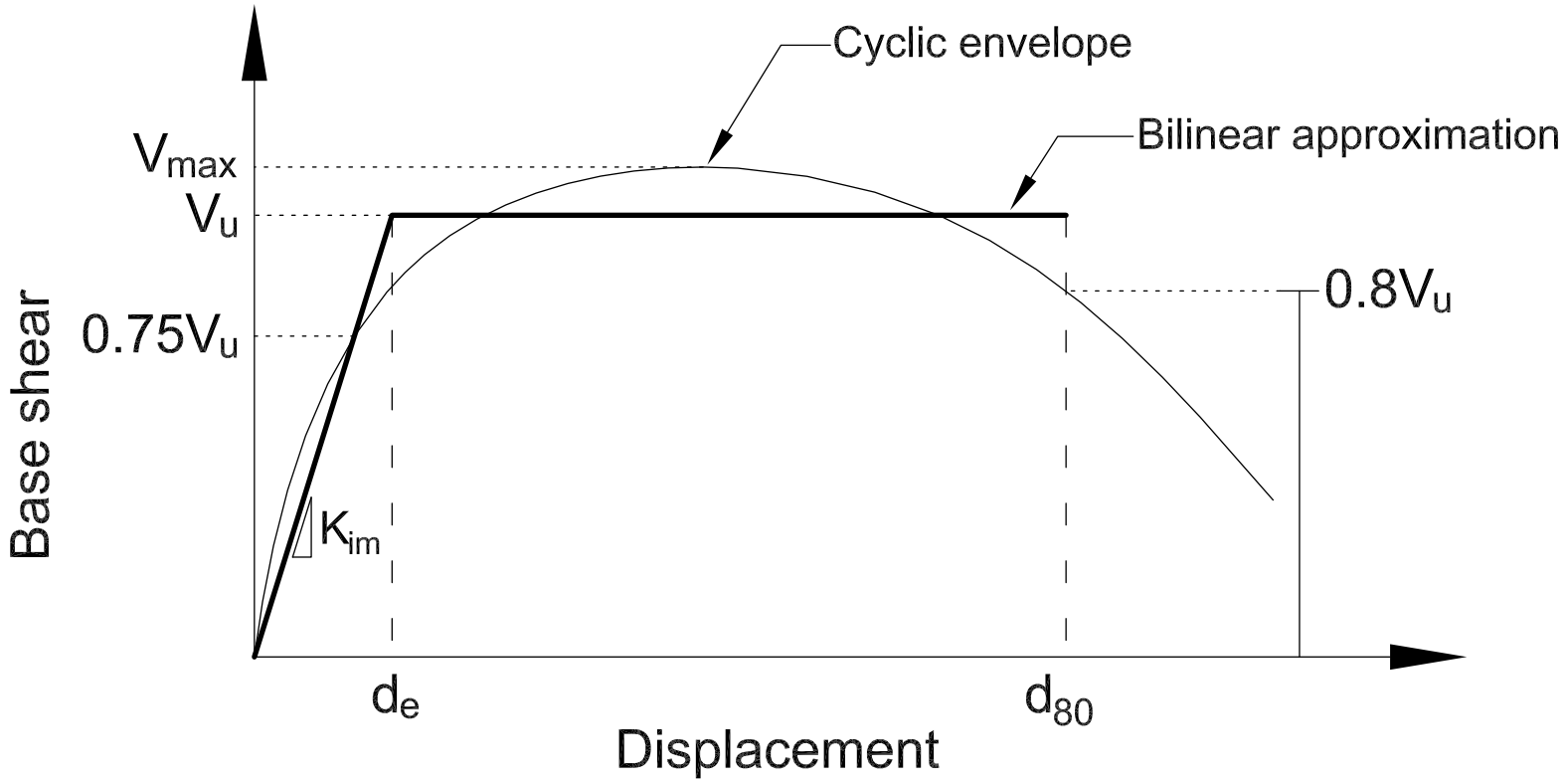

Figure 8a

Journal of Structural Engineering. Submitted April 12, 2011; accepted May 3, 2013;
posted ahead of print May 6, 2013. doi:10.1061/(ASCE)ST.1943-541X.0000863

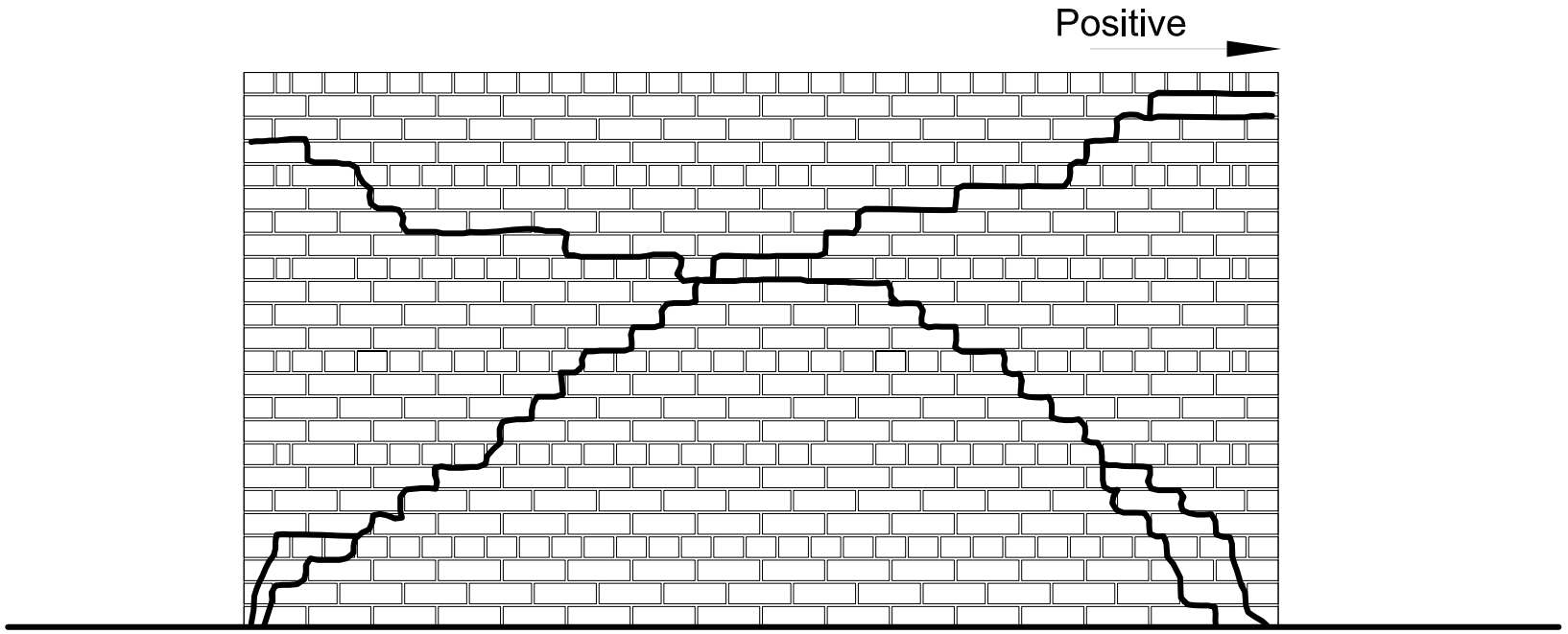

Figure 8b

Journal of Structural Engineering. Submitted April 12, 2011; accepted May 3, 2013;
posted ahead of print May 6, 2013. doi:10.1061/(ASCE)ST.1943-541X.0000863

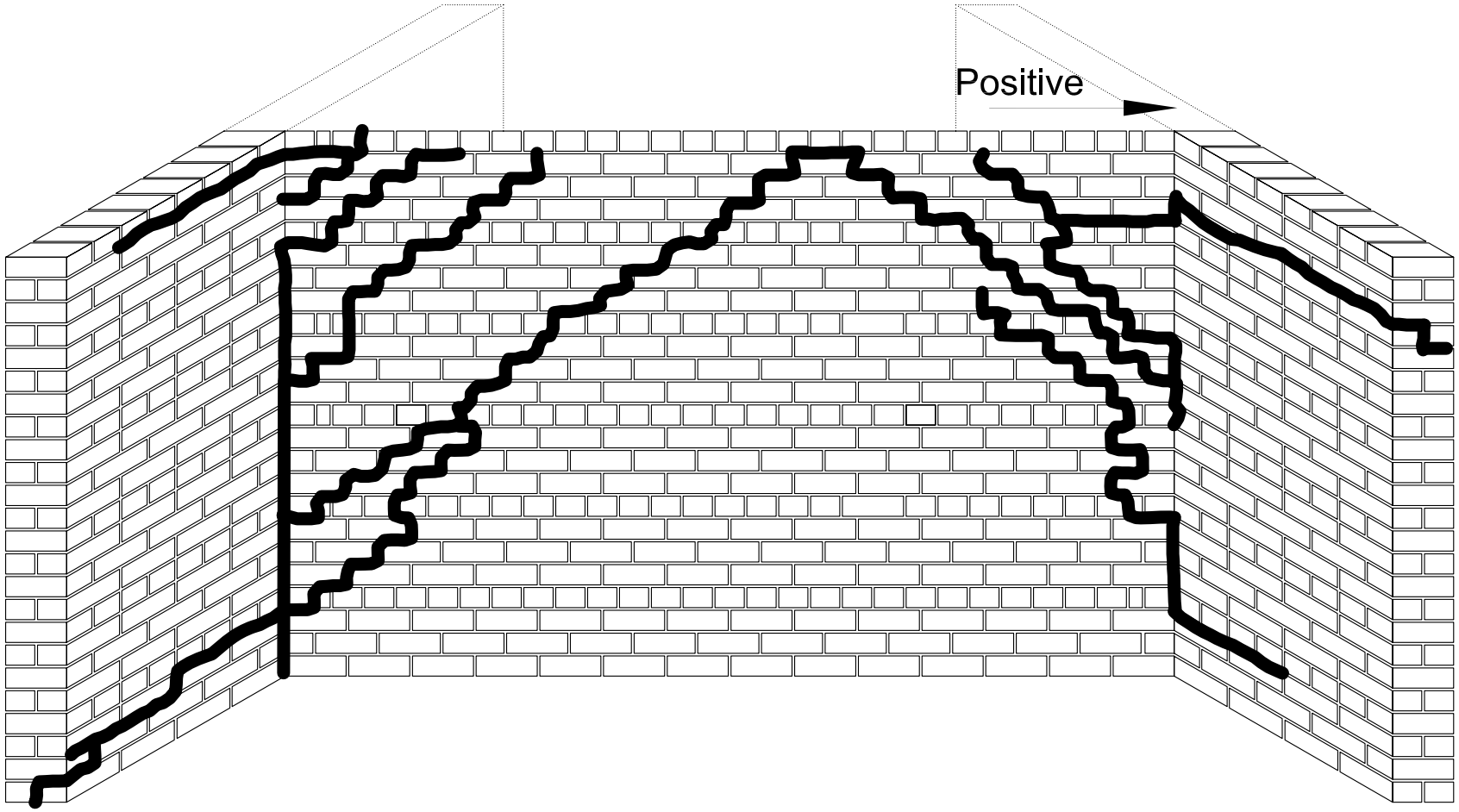

Figure 8c

Journal of Structural Engineering. Submitted April 12, 2011; accepted May 3, 2013;
posted ahead of print May 6, 2013. doi:10.1061/(ASCE)ST.1943-541X.0000863

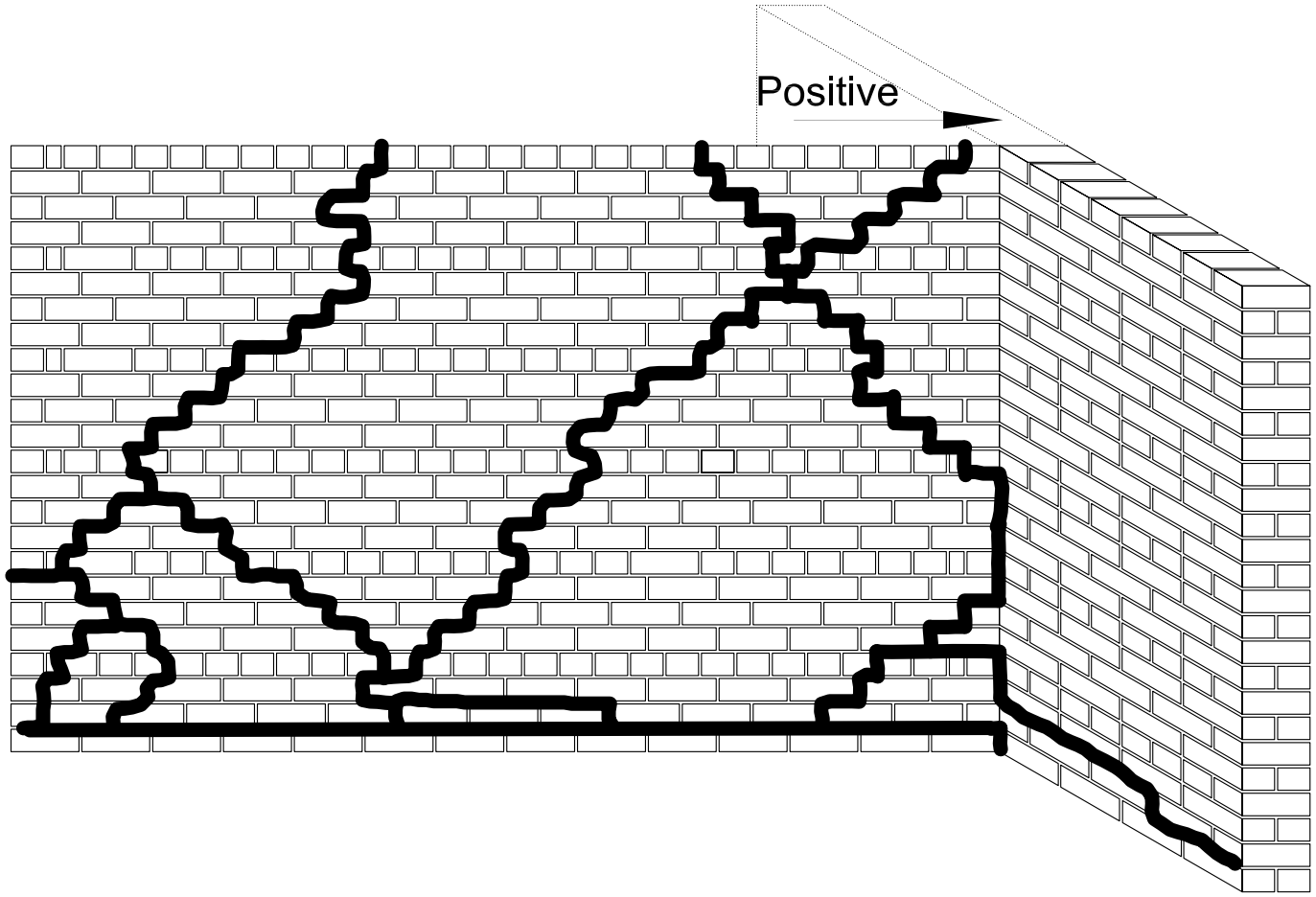

Figure 8d

Journal of Structural Engineering. Submitted April 12, 2011; accepted May 3, 2013;
posted ahead of print May 6, 2013. doi:10.1061/(ASCE)ST.1943-541X.0000863

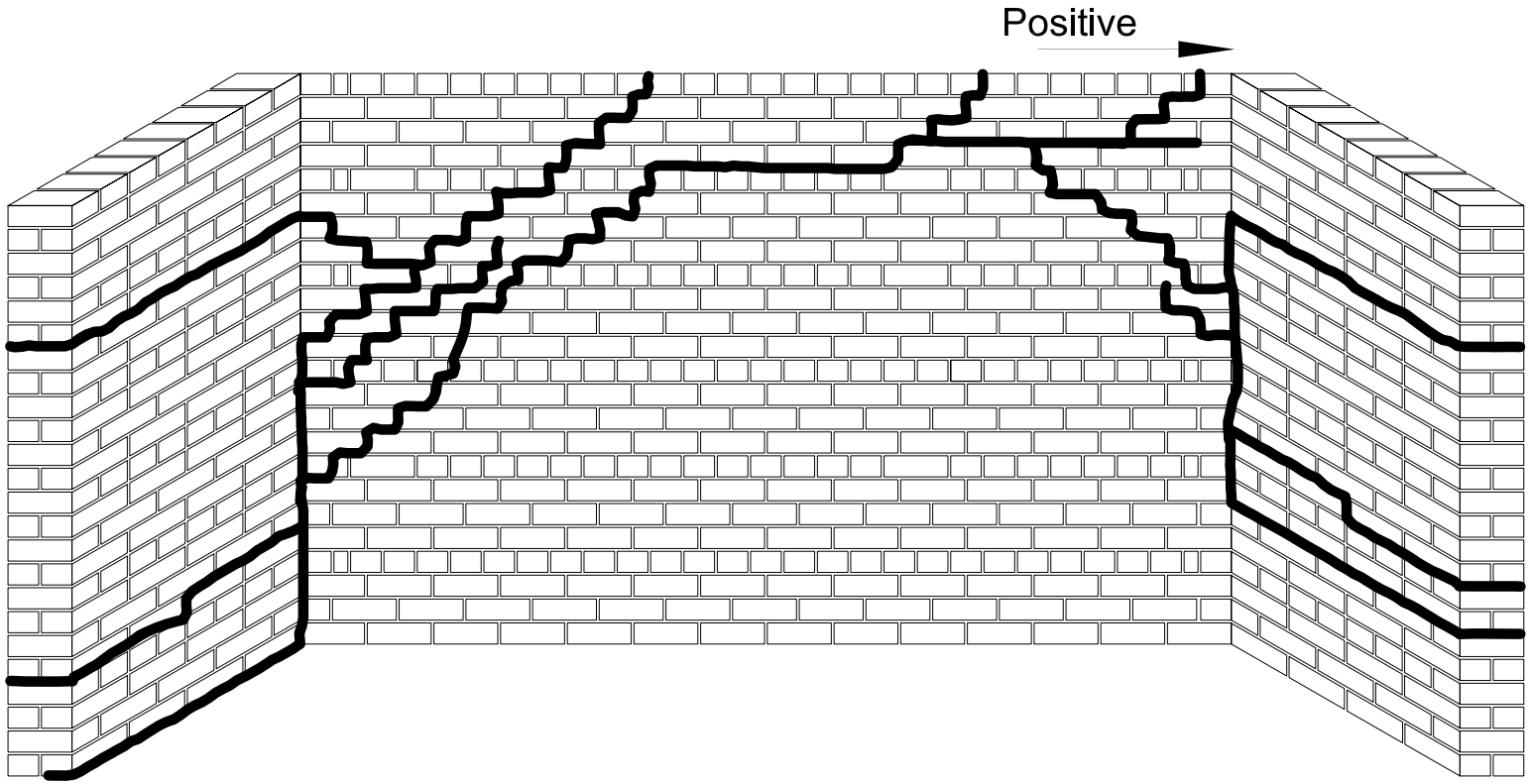

Figure 9a

Journal of Structural Engineering. Submitted April 12, 2011; accepted May 3, 2013;
posted ahead of print May 6, 2013. doi:10.1061/(ASCE)ST.1943-541X.0000863

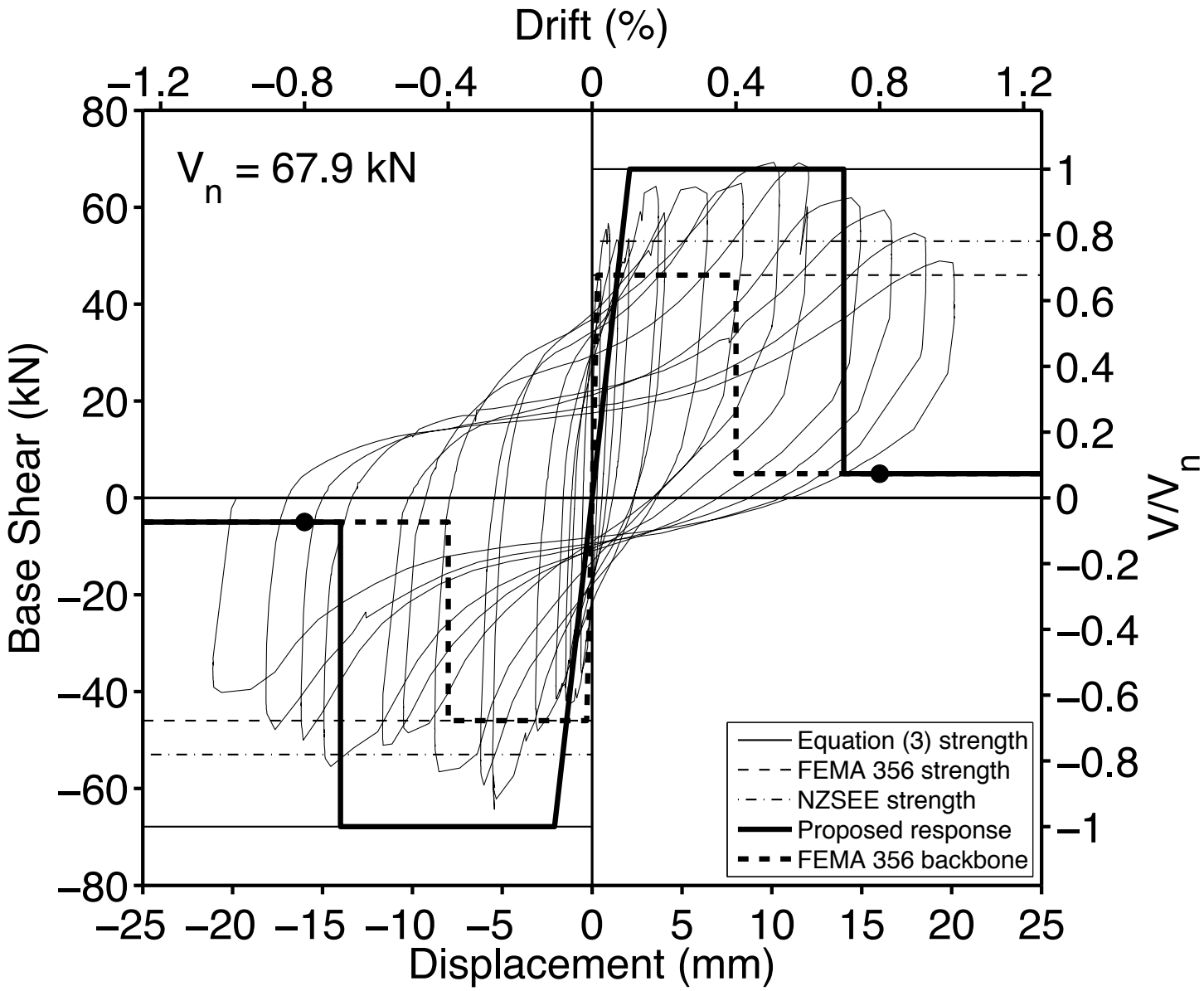

Figure 9b

Journal of Structural Engineering. Submitted April 12, 2011; accepted May 3, 2013;
posted ahead of print May 6, 2013. doi:10.1061/(ASCE)ST.1943-541X.0000863

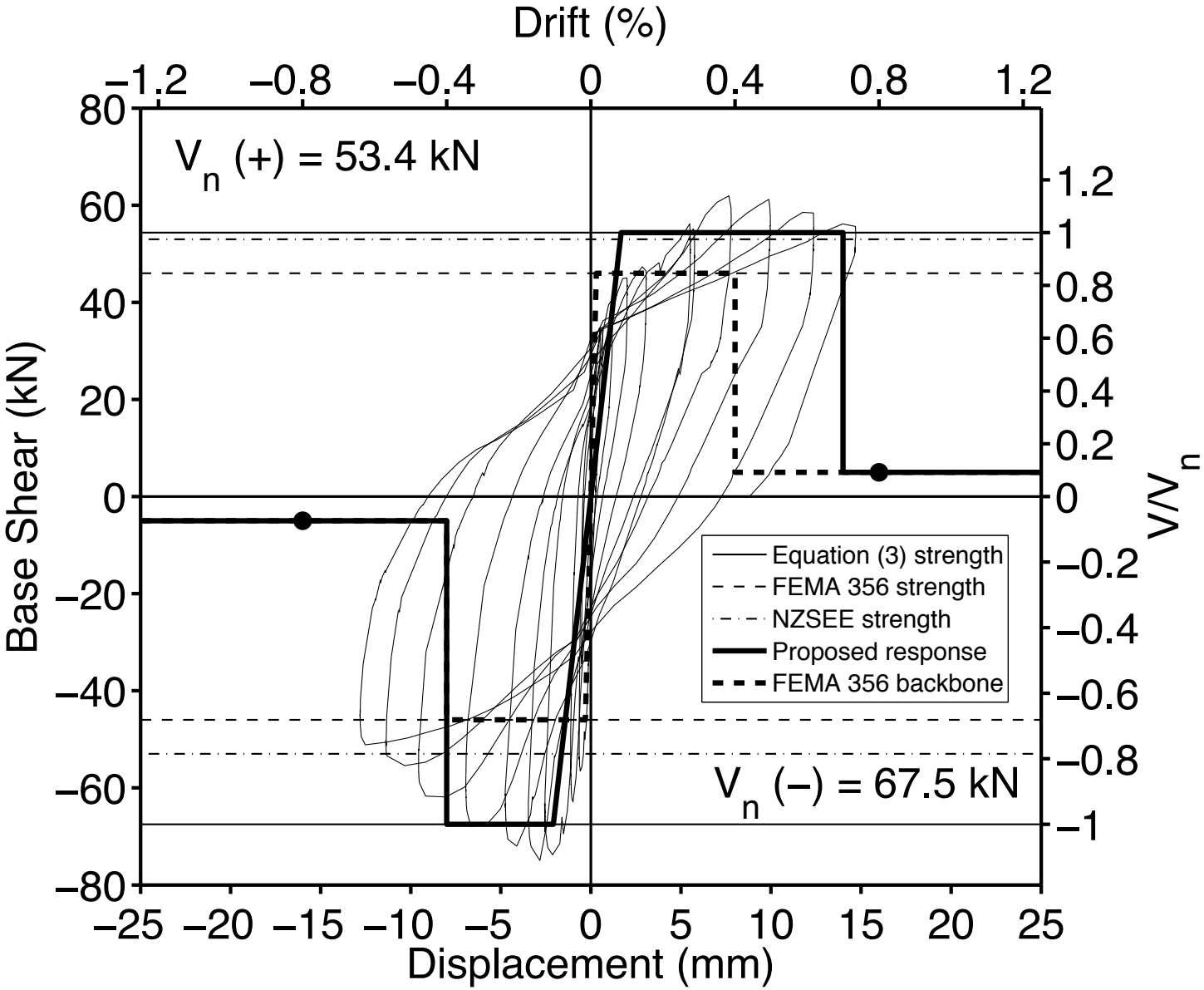

Figure 9c

Journal of Structural Engineering. Submitted April 12, 2011; accepted May 3, 2013;
posted ahead of print May 6, 2013. doi:10.1061/(ASCE)ST.1943-541X.0000863

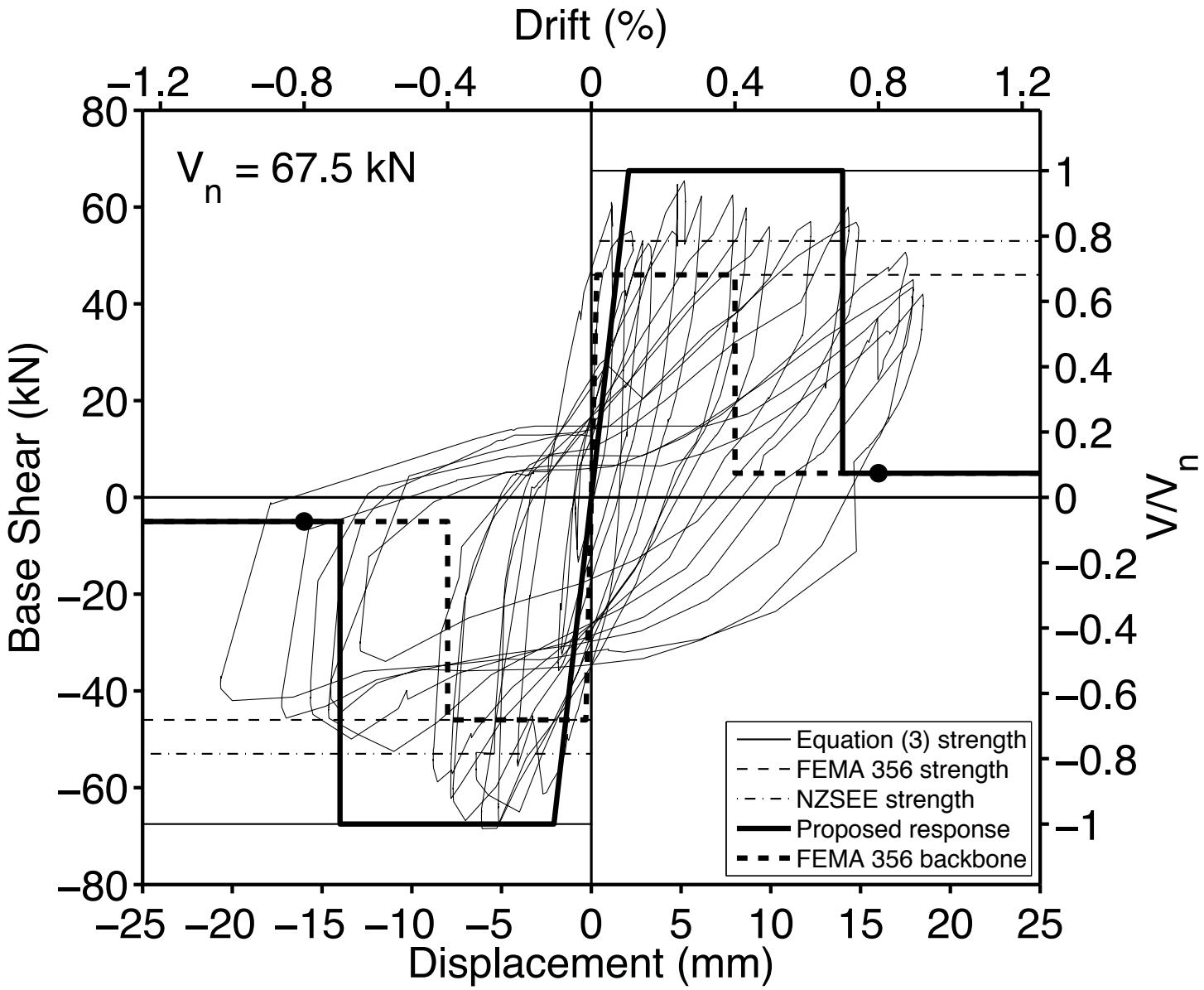

Figure 10

Journal of Structural Engineering. Submitted April 12, 2011; accepted May 3, 2013;
posted ahead of print May 6, 2013. doi:10.1061/(ASCE)ST.1943-541X.0000863

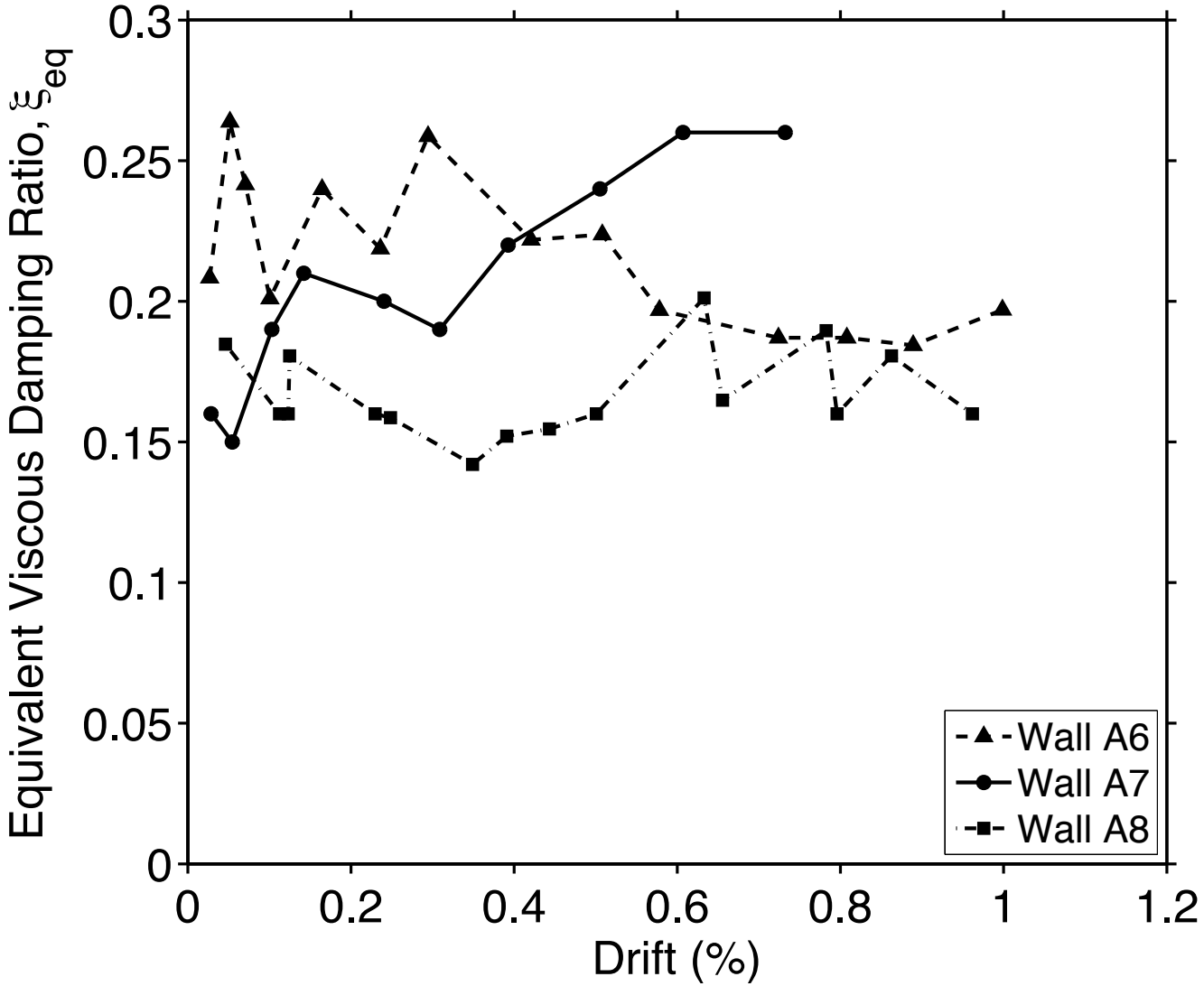

Figure 11a

Journal of Structural Engineering. Submitted April 12, 2011; accepted May 3, 2013;
posted ahead of print May 6, 2013. doi:10.1061/(ASCE)ST.1943-541X.0000863

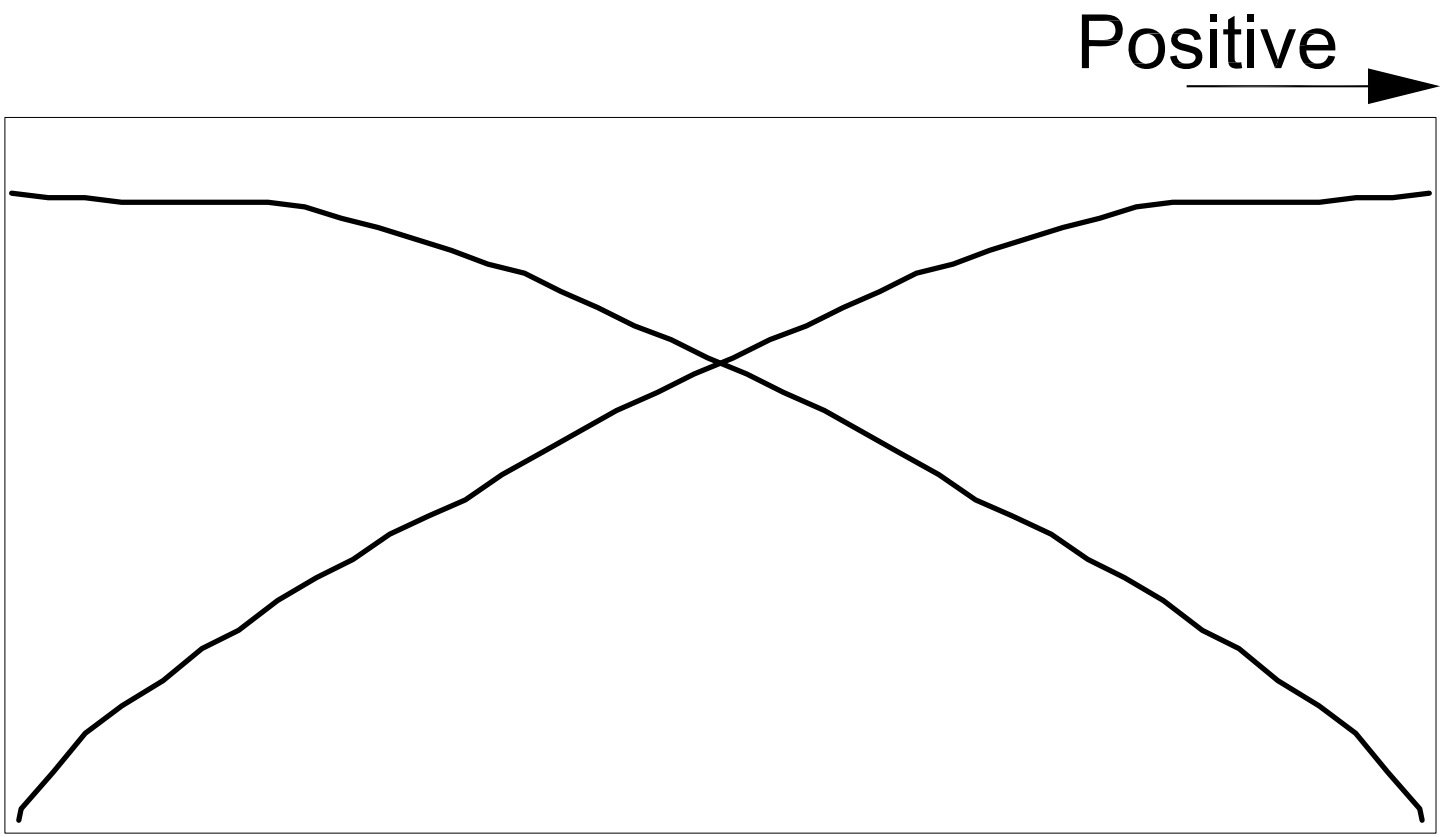

Figure 11b

Journal of Structural Engineering. Submitted April 12, 2011; accepted May 3, 2013;
posted ahead of print May 6, 2013. doi:10.1061/(ASCE)ST.1943-541X.0000863

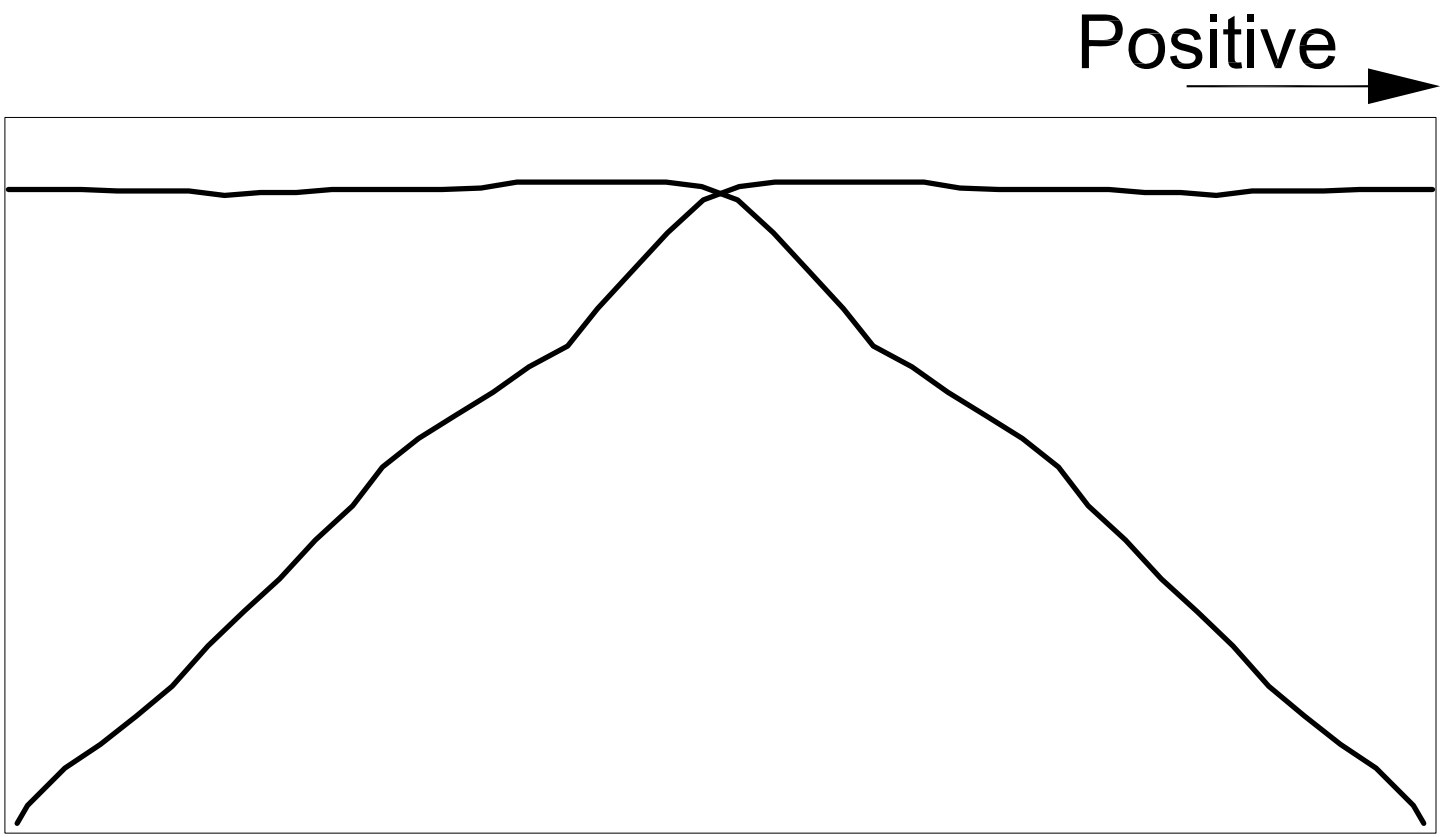

Figure 11c

Journal of Structural Engineering. Submitted April 12, 2011; accepted May 3, 2013;
posted ahead of print May 6, 2013. doi:10.1061/(ASCE)ST.1943-541X.0000863

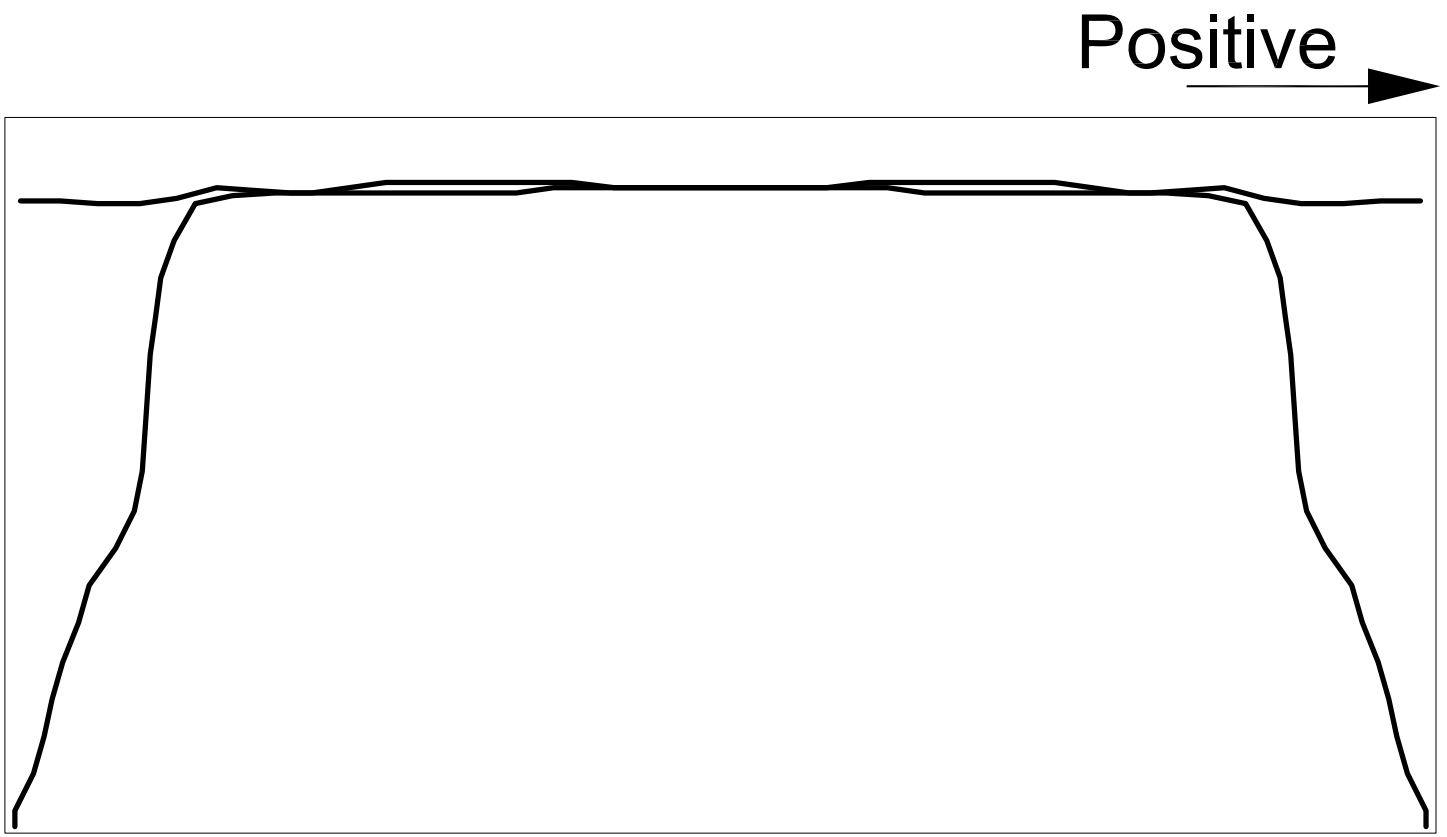

Figure 11d

Journal of Structural Engineering. Submitted April 12, 2011; accepted May 3, 2013;
posted ahead of print May 6, 2013. doi:10.1061/(ASCE)ST.1943-541X.0000863

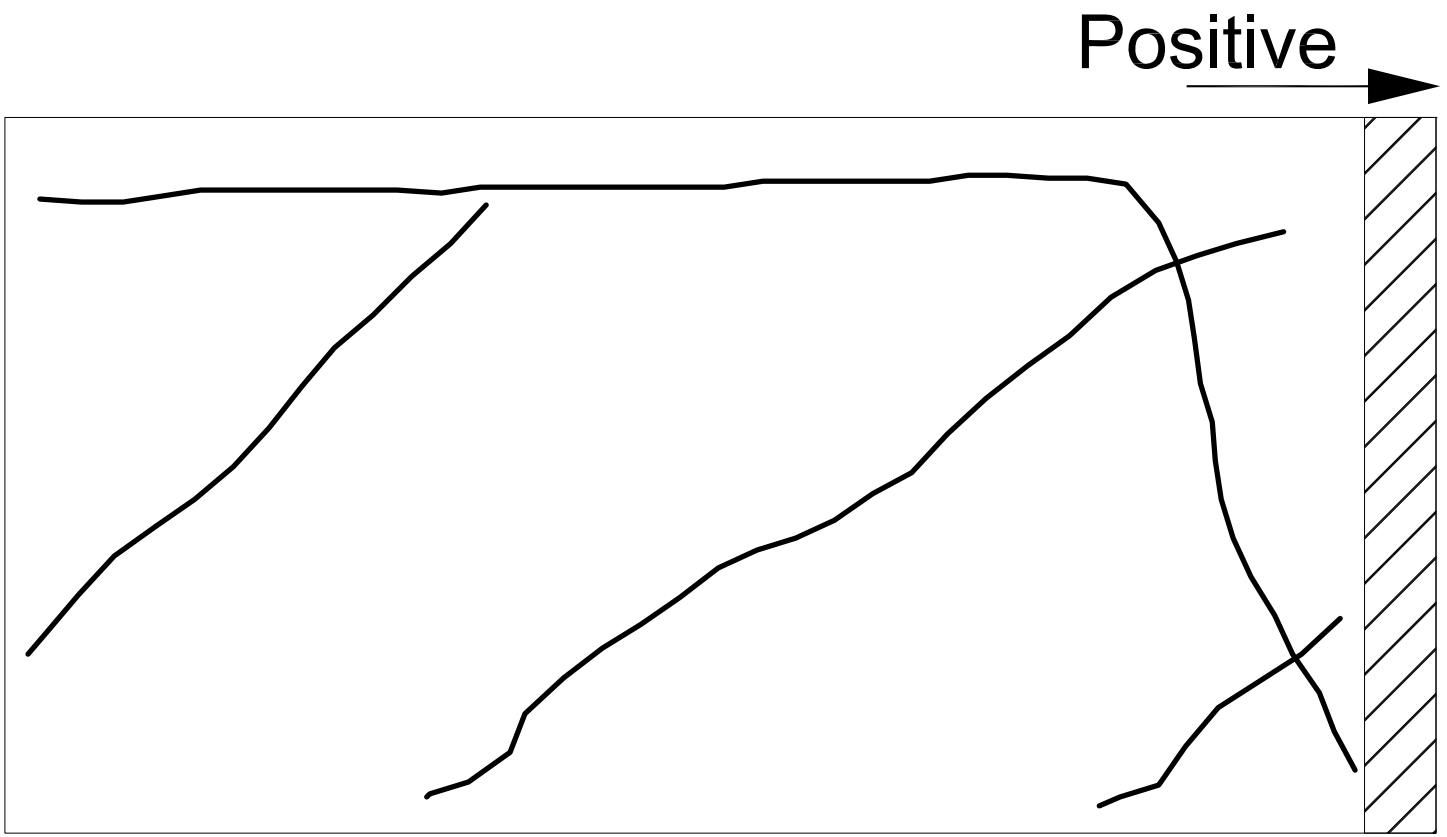

Figure 12a

Journal of Structural Engineering. Submitted April 12, 2011; accepted May 3, 2013;
posted ahead of print May 6, 2013. doi:10.1061/(ASCE)ST.1943-541X.0000863

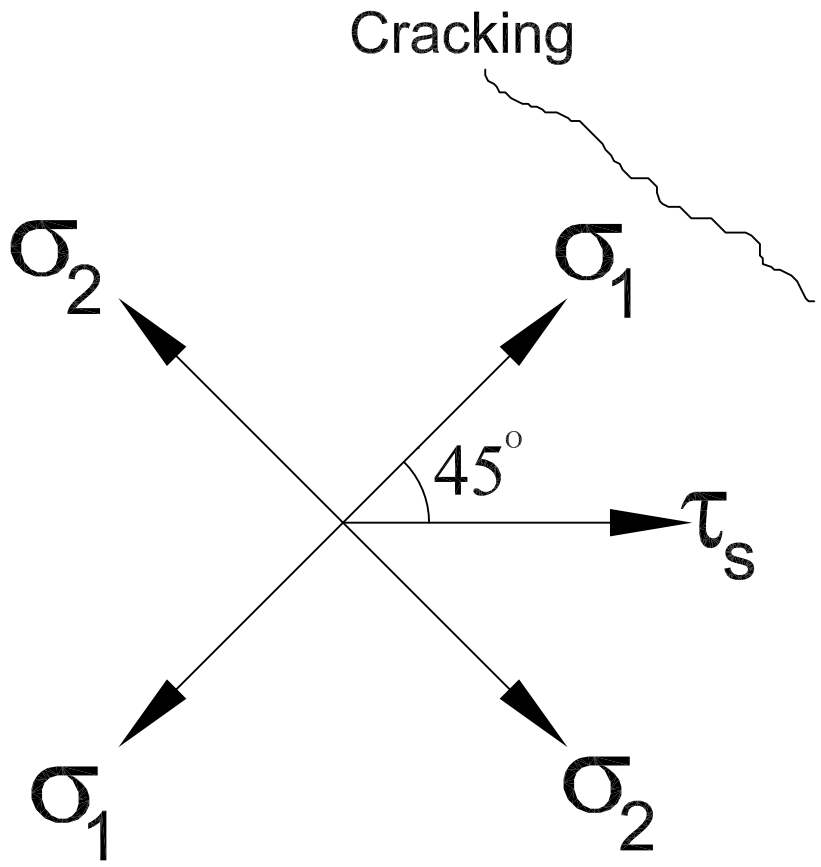

Figure 12b

Journal of Structural Engineering. Submitted April 12, 2011; accepted May 3, 2013;
posted ahead of print May 6, 2013. doi:10.1061/(ASCE)ST.1943-541X.0000863